Infection risk and economic activity trade-offs
decision-making in indoor venue operations for pandemic preparedness

Atamer Balkan, Büşra; Sparnaaij, Martijn; Duives, Dorine; Huang, Yilin; ten Bosch, Quirine

DOI
10.1080/17477778.2025.2546481

Publication date
2025

Document Version
Final published version

Published in
Journal of Simulation

Journal of Simulation

ISSN: 1747-7778 (Print) 1747-7786 (Online) Journal homepage: www.tandfonline.com/journals/tjsm20

Infection risk and economic activity trade-offs: decision-making in indoor venue operations for pandemic preparedness

Büşra Atamer Balkan, Martijn Sparnaaij, Dorine Duives, Yilin Huang & Quirine ten Bosch

To cite this article: Büşra Atamer Balkan, Martijn Sparnaaij, Dorine Duives, Yilin Huang & Quirine ten Bosch (03 Oct 2025): Infection risk and economic activity trade-offs: decision-making in indoor venue operations for pandemic preparedness, Journal of Simulation, DOI: 10.1080/17477778.2025.2546481

To link to this article: https://doi.org/10.1080/17477778.2025.2546481

Published online: 03 Oct 2025.

JOURNAL OF SIMULATION
https://doi.org/10.1080/17477778.2025.2546481

RESEARCH ARTICLE

OPEN ACCESS Check for updates

Infection risk and economic activity trade-offs: decision-making in indoor venue operations for pandemic preparedness

Büşra Atamer Balkan[a], Martijn Sparnaaij[b], Dorine Duives[b], Yilin Huang[c] and Quirine ten Bosch[a]

[a]Infectious Disease Epidemiology, Wageningen University & Research, Wageningen, The Netherlands; [b]Department of Transport & Planning, Delft University of Technology, Delft, The Netherlands; [c]Department of Multi-Actor Systems, Delft University of Technology, Delft, The Netherlands

ABSTRACT

During epidemics, decision-making regarding intervention measures faces complex trade-offs. Interventions targeting indoor venues can mitigate disease spread, since they are associated with higher infection risk for respiratory pathogens. However, as experienced during the COVID-19 pandemic, these measures can lead to economic losses, especially in the hospitality sector. In this study, we propose a hybrid modeling and simulation framework to provide decision support for reducing the infection risk in indoor venues while maintaining viable economic activity. Our framework integrates (i) a microscopic pedestrian model for human movement, (ii) a hybrid simulation model for virus spread and transmission, and (iii) a multi-criteria decision-making approach to identify the best service options. The framework is demonstrated for the SARS-CoV-2 infection risk. The restaurant case study results illustrate that maximizing the distance between seating groups can have a limited effect on the infection risk. Service duration and service capacity are key determinants of expected economic activity, but they constitute significant trade-offs: the former has a substantial impact on the infection risk, and the latter drives the probability of infectious introductions. Our analysis demonstrates the need for multi-criteria approaches during an outbreak and consideration of the epidemiological context for operational decision-making, even at an individual venue.

ARTICLE HISTORY
Received 29 July 2024
Accepted 5 August 2025

KEYWORDS
Agent-based modeling; system dynamics; hybrid model; public health; multi-agent systems; multi-criteria decision-making

1. Introduction & background

In times of public health crises like epidemics, the importance of informed decision-making becomes increasingly evident. From strategic policy formulation to operational implementation, well-designed decision-making processes can save lives, conserve time, and ensure the efficient utilization of available resources. As globally experienced in COVID-19 pandemic, decision-makers require readily available tools to address diverse decision-making challenges (Panovska-Griffiths et al., 2021), and mathematical modeling and simulation approaches can strengthen our pandemic preparedness (Hutton, 2013; Silal, 2021; Singh & Mathirajan, 2023) by enabling quantitative assessments of possible responses to such complex problems.

The challenge of decision-making problems in the context of disease outbreaks mostly stems from the complicated trade-offs they include: The need to control the infections can lead to lockdowns and stay-at-home orders, which have a clear impact on income, education, and social lives (Filipe et al., 2022). During the recent pandemic, stakeholders in specific sectors where social interactions occur, such as hospitality, catering, food, and entertainment tried to maintain their financial sustainability by adjusting their operations while adhering to necessary safety measures like limiting the occupancy levels and service durations (Brizek et al., 2021; Gursoy & Chi, 2020; Norris et al., 2021). For the safe and economically viable use of public venues in case of epidemics, there is a need for multi-dimensional and adaptable intervention schemes that consider both public health and socio-economic impacts (Eryarsoy et al., 2023). However, what level of interventions is acceptable —considering both the infection risk safety and economic sustainability—still remains an unresolved question that varies by context and is affected by different epidemiological scenarios.

In the context of epidemics and pandemics, simulation modeling approaches have been widely used for different decision-making challenges including design of social distancing measures (Volpatto et al., 2023), timing and impact of public health restrictions (Duggan et al., 2024), understanding the impact of vaccination policies (Vázquez-Abad et al., 2022), investigating the influence of behavioral interventions on the spread of the disease for large populations (de Mooij et al., 2023), supporting local

CONTACT Büşra Atamer Balkan busra.atamerbalkan@wur.nl Infectious Disease Epidemiology, Department of Animal Sciences, Wageningen University & Research, P.O. Box 338, 6700 AH Wageningen, The Netherlands

decision-makers for pandemic preparedness (Araz et al., 2011), vaccine prioritization, allocation, and rationing (B. Y. Lee et al., 2010) and managing supply chain risks (Ivanov, 2020). In addition to the discrete event simulations widely used in health system operations and resource management (Currie et al., 2020), and system dynamics models typically utilized to capture the population-level spread of the disease, the use of agent-based models has gained more attention since they enable researchers to simulate individual behavior and interactions (Dunke & Nickel 2021). Some agent-based modeling studies have investigated the effects of interventions on SARS-CoV-2 transmission risk in various social contexts (Kerr et al., 2021; Müller et al., 2021; Zhou et al., 2021), primarily aiming to provide community-level insights rather than facilitate operational decision-making. Additionally, hybrid simulation studies (Brailsford et al., 2019; Mustafee et al., 2025; Nguyen et al., 2024) that combine different simulation methods are increasingly common for decision-making in infectious disease contexts (e.g., Angelopoulou & Mykoniatis, 2024; Viana et al., 2014) since hybrid approaches can facilitate a more robust decision-making process (Kar et al., 2024) in complex health problems.

In addition to their methodological differences, these simulation studies show diverse characteristics in terms of how they approach the trade-offs: the majority of them focus on a single outcome to improve, while some of them are more comprehensive considering multiple objectives (e.g., Alım & Kesen, 2023; Araz, 2013; Dunke & Nickel, 2021). The latter group utilizes multi-criteria decision-making approaches, generally focusing on improved design of population-level intervention policies, such as the optimal timing of the lockdown policies or the country-level rollout of mitigation regulations (Chandak et al., 2020; Chen et al., 2023; Colas et al., 2021; Gillis et al., 2021). However, understanding the multi-faceted impacts of these interventions at the scale of an individual venue, where the interactions occur between individuals and hence the infection happens, is crucial. For the case of SARS-CoV-2, indoor gatherings have been linked to an eighteen times larger risk of transmission compared to outdoor gatherings (Bulfone et al., 2021), which indicates the importance of decision support for intervention design in indoor spaces in mitigating the infectious diseases caused by respiratory pathogens.

To understand the impact of interventions on the virus transmission dynamics in indoor spaces, diverse mathematical modeling and simulation approaches are utilized, and an overview of indoor transmission models can be found in Atamer Balkan et al. (2024). In terms of understanding the multidimensionality of the infection risk in different indoor settings, agent-based and hybrid simulation models with varying levels of detail on mobility and the spread of the virus (Islam et al., 2021; B. Lee et al., 2021; Martinez et al., 2022; Xiao et al., 2021; Ying et al., 2021; Zhu et al., 2025) have contributed to the knowledge base. In addition to those, many mathematical modeling studies investigate the optimal design of indoor spaces to mitigate the infection risk, mainly focusing on minimizing the distance between customers/sitting groups/tables, since the maximum distance is accepted as an indicator of minimum transmission risk (Bortolete et al., 2022; Contardo & Costa, 2022; Fischetti et al., 2021; Moore et al., 2021; Ntounis et al., 2020; Ugail et al., 2021). However, limited research focused on short-term operational decision-making problems on how to operate a particular venue in terms of service options (e.g., the number of guests allowed, the duration of the service, the number of shifts) that the venue managers could implement themselves to manage a key trade-off: reducing the transmission risk while maintaining sustainable economic activity. Addressing this gap, our research questions in this study are as follows.

- What are the impacts of different service options on respiratory virus transmission risk in an indoor venue? (Sections 3.1–3.3)
- How can the best service options be identified that keep the transmission risk below an acceptable threshold, while maintaining sufficient economic activity? (Section 3.4)
- How does the infection prevalence within a community impact the set of best service options? (Section 3.5)

To address these research questions, we propose a hybrid modeling and simulation framework that assesses both the transmission risks and the expected economic activity in conjunction and identifies the set of best service options for the safe and economically sustainable use of the space. Our framework uses an integrated set of mathematical models: (i) an agent-based, pedestrian mobility simulation model that captures human activity choices and movement dynamics, (ii) an integrated hybrid simulation model that computes the infection risk of each agent, with agent-based components for virus transmission, and system dynamics components for the virus spread in the environment, and (iii) a multi-criteria decision-making stage to identify the trade-off between the expected daily economic transactions and the infection risk. Our framework is applicable to respiratory pathogens in general that spread through multiple transmission routes (i.e., aerosols, droplets and surfaces). In this paper, we demonstrate its application using SARS-CoV-2 as a case study. The integration of models mentioned in (i) and (ii) is titled Pedestrian

Dynamics—Virus Spread model (PeDViS) and is detailed in Atamer Balkan et al. (2024). PeDViS is calibrated with respect to human mobility data in indoor public spaces and utilizes up-to-date virological and epidemiological data on SARS-CoV-2. It has gone through relevant model validation and verification stages (Appendix F), and the parametrization and the sensitivity analysis of PeDVis are presented in detail in Atamer Balkan et al. (2024).

In this study, we showcase the application of our hybrid model for restaurants. Restaurants, especially indoor dining, have been identified as one of the highest risk settings during COVID-19 pandemic (Fisher et al., 2020), mostly attributable to the low mask-wearing rate for eating and drinking, contact for prolonged periods of time, possible high occupancy, possible poor ventilation, and limited adherence to social distancing rules (Fisher et al., 2020; Li et al., 2021; N. Zhang et al., 2021). In this study, we consider the viewpoint of an indoor venue manager and aim to make a comparative analysis of the interventions that are related to operating the restaurant from an indoor venue manager's perception. In addition to the redesign of the physical space, we assess the contribution of different service options (namely, the service duration, the service capacity, and the service scheme in our restaurant case) regarding the infection risk and the expected daily economic transactions. This study constitutes one of the first investigations of decision-making at the scale of an individual indoor venue considering both the economic sustainability and infection risk safety concerning a respiratory pathogen.

2. Hybrid model framework

In this section, we introduce our hybrid model that combines PeDViS with multi-criteria decision-making. First, the relevant setting for an indoor venue (i.e., a restaurant) is introduced (Section 2.1) with key assumptions related to virus dynamics in the environment. Then, the Pedestrian Behavior and Movement module (Section 2.2.1) and QVEmod module (Section .2) are presented with the assumptions about the economic activity in an indoor venue (Section .3) and the multi-criteria decision-making approach followed (Section .4). Additionally, the model validation and verification stages are summarized in Appendix F.

2.1. The setting: Layout and elements of an indoor venue

Considering human movements and interactions within an indoor environment, the attributes of the space include context-based infrastructural elements (e.g., walls, entrance, exit, kitchen, bar, restroom) and movable objects (e.g., tables and chairs) specific to that setting (i.e., a restaurant in our case study). The layout of the space can be perceived as a collection of layers where infrastructural elements and movable objects are placed, the individuals move and perform actions, and the virus spread occurs (Figure 1).

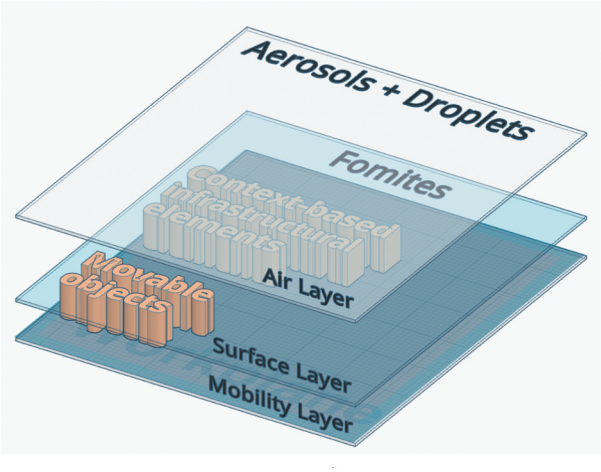

Figure 1. Layers in the layout.

In this study, the default layout is rectangular and carries three layers of information with small units of grid cells (Figure 2). The human movements and actions are performed on the mobility layer on a continuous space, then the mobility information is converted to a discretized space (with grid cell sizes of 0.2 m × 0.2 m), while the virus spread information in the environment is tracked on the air and the surface layers (with grid cell sizes of 0.5 m × 0.5 m) (Figure 1).

The virus spread information on the air and surface layers are used to track the virus transmission routes between agents and the environment. Virus exposure by agents occurs by acquiring viral particles via direct or indirect contact with an infectious individual. The transmission (i.e., the process of virus exposure which results in infection) and the spread of respiratory

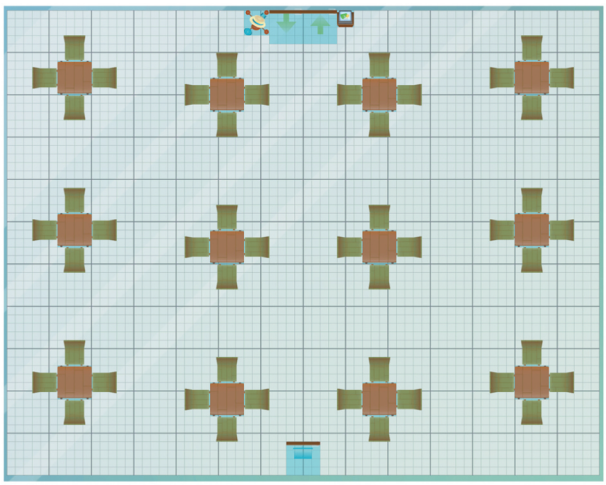

Figure 2. An example restaurant setting including the grids on the mobility layer.

viruses like SARS-CoV-2 can typically occur through three routes: (i) droplets (i.e., large viral-laden particles (size >10um) that fall to the ground rapidly), (ii) aerosols (i.e., small viral-laden particles (size <10um) that can remain airborne for a period of time), and (iii) fomites (i.e., when contaminated surfaces act as intermediary vectors to cause virus exposure when individuals touch them) (Atamer Balkan et al., 2024). In our model, the air layer includes information for the virus accumulation in the form of aerosols and droplets, whereas the surface layer contains the information for fomites.

In many infectious diseases, especially those whose transmission through surfaces plays a major role such as Ebola or chickenpox, shared surfaces can be an important infection transmission route. PeDViS can also simulate the virus transmission mechanism through surfaces along with the aerosols and droplets and is thereby generic in representing all transmission routes relevant to respiratory pathogens. However, for the case of COVID-19, evidence shows that the virus mainly spreads through respiration (Greenhalgh et al., 2021; Miller et al., 2021; R. Zhang et al., 2020), and transmission through surfaces is limited (Cheng et al., 2022; Lewis, 2021; N. Zhang et al., 2021). Experimental studies have shown that SARS-CoV-2 can be transmitted through the environment (Gerhards et al., 2023), but this transmission is mostly related to a build-up of the virus resulting from a prolonged residence time in a shared environment (i.e., the cumulative deposition of droplets over time), rather than through high touch surfaces. Therefore, for this particular simulation, the surface transmission route is considered only through the main activity areas of the customers, which are their *tables* and *chairs*.

Infrastructural elements and movable objects exist in two layers: in the mobility layer they define the constraints for movement (e.g., entrance to the venue can be done only via the front door); in the surface layer they act as a medium for virus transmission between agents (Figures 1 and 2).

The model setup also includes Agents moving around the space. Each agent can either be a *guest* or *service personnel*, which impacts their activities and mobility behavior (Section 2.2.1). An agent can either be *infectious* (i.e., an individual who can spread the virus) or *susceptible* (i.e., an individual who can be infected if exposed to sufficient virus particles) concerning their infectiousness status with the virus. The status of an agent (*infectious* or *susceptible*) defines their virus-transmission-related actions during their visit (e.g., *virus emission* can only be triggered by an *infectious* agent) (Section .2). Additional assumptions about the model structure are given in Appendix A.

2.2. The hybrid model framework

Our hybrid framework (Figure 3) starts with the *Pedestrian and Mobility* module (Section 2.2.1). The first model in that module, *Activity Choice and Scheduling*, transforms user inputs about context, layout and population into personalized activity

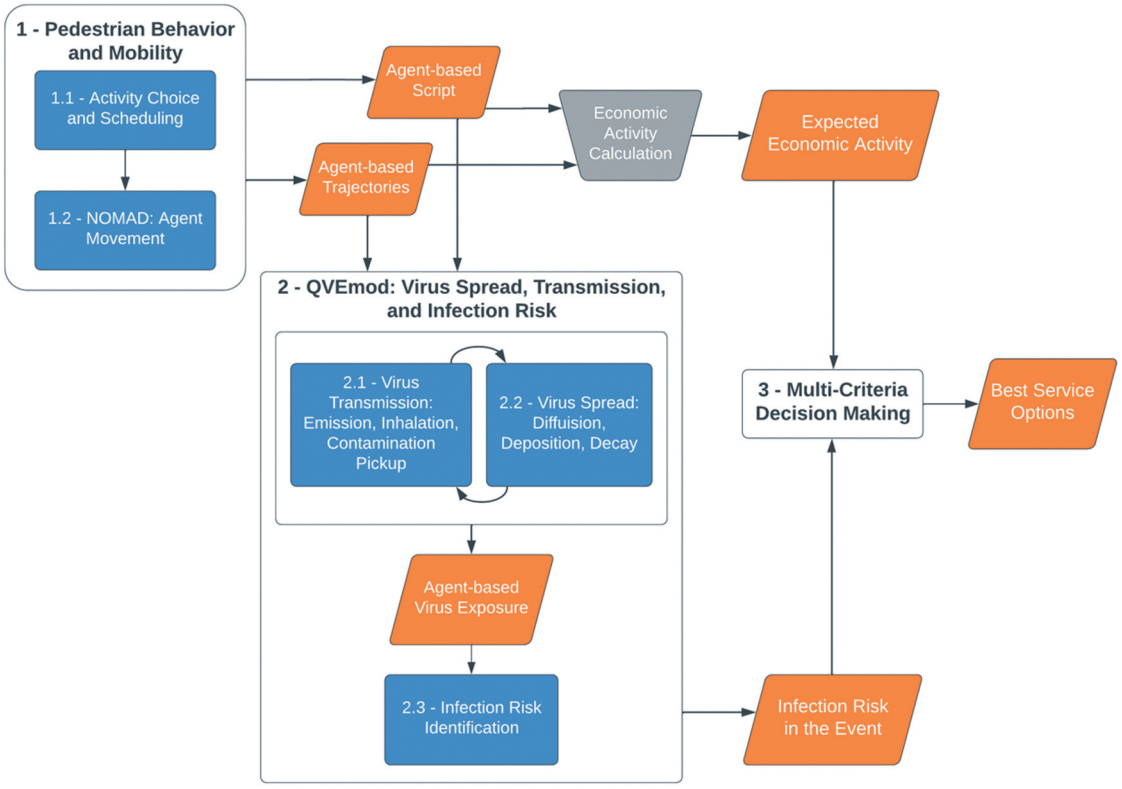

Figure 3. Overview of the hybrid model framework.

schedules (Section .1). The second model, *NOMAD: Agent Movement*, uses these schedules to determine each agent's movement behavior (Section .2). The expected *Economic Activity Calculations* are primarily based on the time spent at the venue, as determined by each agent's entrance and leave times (Section .3). The following module, *QVEmod*, simulates how the respiratory pathogen spreads: it combines an agent-based model (*2.1 – Virus Transmission* in Figure 3), which tracks interactions and virus transmission between agents (Section 2.1), with a system dynamics simulation (*2.2 – Virus Spread* in Figure 3), which tracks the concentration of the viral particles in the environment (Section 2.2). Then, the *Infection Risk Identification* model calculates each agent's infection risk based on viral exposure (Section 2.2.2.3). Finally, in the *Multi-Criteria Decision-Making* stage, we evaluate the best set of service options considering both the expected infection risk and economic activity using Pareto optimality principles (Section .4). Underneath, a detailed explanation of the modeling steps is provided.

2.2.1. Pedestrian behavior and mobility

The *Pedestrian Behavior and Mobility* section of the framework consists of two parts (Stages 1.1 and 1.2 in Figure 3). First, the *Activity Choice and Scheduling* model determines the order of the activities and activity locations that an agent visits during the simulation. Second, the *Agent Movement (NOMAD)* model simulates the trajectory of agents while navigating through the restaurant. These two models require (1) the layout of the restaurant, (2) the duration of the simulation, (3) the demand pattern (i.e., how many groups of customers visit the restaurant during which time slots), (4) the average service duration (i.e., the average duration of group visits), (5) the number of service personnel, (6) the average number of servings per table (i.e., the average number of times the personnel visits a group) and (7) the serving neighborhoods (i.e., the set of tables that is primarily served by specifically assigned members of the personnel) as inputs.

2.2.1.1. Activity choice and scheduling. The agent-based activity choice and scheduling model (1.1 in Figure 3) schedules the activities for the guests and the personnel. For each *guest*, the model creates a static activity schedule at the start of the simulation with three mandatory activities: entering the restaurant, sitting at the table, and leaving the restaurant. Next, optional activities are assigned to the itineraries, such as, visiting the coat rack, visiting the restroom, and paying at the table or the register. In the activity scheduler, the entrance time and the visiting duration of the customers, and the probability of visiting the restroom introduce variability in agent behavior. For the *personnel*, the model creates and assigns the relevant activities (i.e., welcoming and distributing the menus, taking orders, serving orders, receiving payments, cleaning) dynamically during the simulation. For a detailed description of the activity choice and scheduling model, the reader is referred to Sparnaaij et al. (2024).

2.2.1.2. NOMAD: Agent movement. The agent-based movement model in our hybrid framework (1.2 in Figure 3) is an existing microscopic pedestrian simulation model called NOMAD (Campanella, 2016). The NOMAD model computes the route and operational movement dynamics of each pedestrian in the restaurant. The routes are computed such that an agent will choose the shortest route to their destination whilst keeping a comfortable distance to all obstacles.

The operational movement dynamics of the agents are governed by the so-called social forces. The equations governing the operational movement dynamics of each pedestrian are provided in Appendix B. The walking behavior of the population is assumed to be homogeneous in movement aspects, except for the desired walking speed, which is drawn from a normal distribution for each agent.

The pedestrian behavior and mobility model outputs detailed data on the movements and activities of all agents. For each agent, the position is recorded every 0.1 seconds resulting in a detailed trajectory per agent. These outputs are converted into the inputs of the *QVEmod: Virus Spread, Transmission, and Infection Risk Identification* model in the form of a script for each agent after the conversion of the time step from 0.1 seconds to a user-defined value (default = 30 seconds). A simplified example script for one agent is provided in Appendix C.

2.2.2. QVEmod: Virus spread, transmission, and infection risk

Given the context-based infrastructural elements, objects, layout, and the agent-based script and routing information, how would a respiratory pathogen spread in an indoor venue and transmit between agents if one of the agents were infectious? We approach this question with a hybrid simulation model (QVEmod) integrating (1) an agent-based simulation tracking the interaction of each agent with the virus (Stage 2.1 in Figure 2) and (2) system dynamics simulation tracking the virus spread in the environment (Stage 2.2 in Figure 2). These two simulations run simultaneously with the same time steps (i.e., 30 seconds), feeding each other information in each time step.

The processes modeled in QVEmod are summarized here and detailed in Appendix D. A causal loop diagram showing the relationships between the processes in QVEmod and the viral particles in the

environment is provided in Appendix E. After the run is concluded, the infection risk in this event for each agent is calculated (Stage 2.3 in Figure 3) as one of the primary outputs of our framework.

2.2.2.1. Agent-based simulation for virus transmission. The agent-based module of QVEmod simulates the virus transmission-related processes performed by agents throughout the simulation. At the start of the simulation, one agent is randomly assigned as *infectious*, and the rest of the visitors are labeled as *susceptible*; this constitutes the main source of randomness in QVEmod. As the *infectious agent* enters the space, two biological processes are triggered:

- With *virus emission*, the infectious agent emits viral particles to the air within aerosols and droplets (Eqs. A7 and A8).
- During *surface contamination*, the infectious agent touches and contaminates the surfaces within their reachable area with a surface contamination rate (Eqs. A9 and A10).

After the infectious agent enters the space, the model starts calculating the interactions of the *susceptible agents* with the virus via these two processes:

- With *virus inhalation*, the susceptible agents are exposed to the virus via the viral particles in aerosols and droplets in the air layer (Eqs. A11 and A12).
- During *virus pickup from the surfaces*, the susceptible agent can touch contaminated surfaces and pick up the virus onto their hands with a virus pick-up rate, and then transfer them to their facial membranes (Eqs. A13, A14 and A15).

As a result of these biological processes, the susceptible agents get exposed to the virus. The virus exposure amount of each susceptible agent is calculated for each route: virus exposure via aerosols, droplets, and fomites.

2.2.2.2. System dynamics simulation for virus spread in the environment. While the agent-based module triggers and calculates the biological processes performed by the agents, the system dynamics module dynamically tracks the concentration of virus particles within the environment. The stock variables in the module represent the virus accumulation in each grid cell (x, y): $V_{aerosols}\ (x, y)$, $V_{droplets}\ (x, y)$, and $V_{fomites}\ (x, y)$. In addition to the agent-based processes explained above, there are three agent-independent flow variables in the environment.

- The viral particles in the environment follow an exponential decay and lose their infectivity in time with virus decay rates for aerosols and droplets (Eqs. A19 and A20).
- Different from the virus decay in aerosols and fomites, the particles in droplets fall onto surfaces: they are transferred from grid cell (x, y) in the air layer to grid cell (x, y) in the surface layer with a droplet deposition rate. The droplet deposition process is much faster compared to the decay process, so any decay in droplets is ignored (Eq. A21).
- The virus particles in the air layer diffuse into their neighborhood grid cells in x and y directions with diffusion rates for aerosols and droplets (Eqs. A22 and A23).

As a result of the flows triggered by the biological processes of agents and other virus-spread-related processes in the environment, the virus contamination state of each layer, for each grid (x, y) and for each time step, is calculated (Figure 4) (Eqs. A24, A25 and A26). The details of the calculations are provided in Appendix D.

2.2.2.3. Infection risk identification. After the agent-based and system dynamics simulation runs are completed, the model uses the agent-based virus exposure information and quantifies the infection risk for each susceptible agent via the exponential dose–response relationship (Nicas, 1996).

$$P^s = 1 - e^{-\left(\frac{E^s{}_{aerosols}(T)}{k_{aerosols}} + \frac{E^s{}_{droplets}(T)}{k_{droplets}} + \frac{E^s{}_{fomites}(T)}{k_{fomites}}\right)} \quad (1)$$

Here, P^s is the probability of infection for susceptible agent s, where $E^s{}_{aerosols}(T)$, $E^s{}_{droplets}(T)$, and $E^s{}_{fomites}(T)$ are the accumulated virus exposure amounts for the susceptible agent s via each route at the end of the simulation duration, T. $k_{aerosols}$, $k_{droplets}$ and $k_{fomites}$ are the route-specific exposure parameters (Popa et al., 2020; Atamer Balkan et al., 2024). The details of exposure calculations are provided in Appendix D.

Then the infection risk of the event is calculated by summing up the infection risk for each agent $s \in S$. This summation represents "the expected number of secondary infections given the introduction of one infectious agent", and hence it corresponds to what we will refer to as the reproduction number attributed to this event, R_{event}.

$$R_{event} = \sum_{s=1}^{s=S} P^s \quad (2)$$

2.2.3. Economic activity

The expected economic activity in an event or a day, which is the expected revenue in our example, depends on the visit characteristics of the guests.

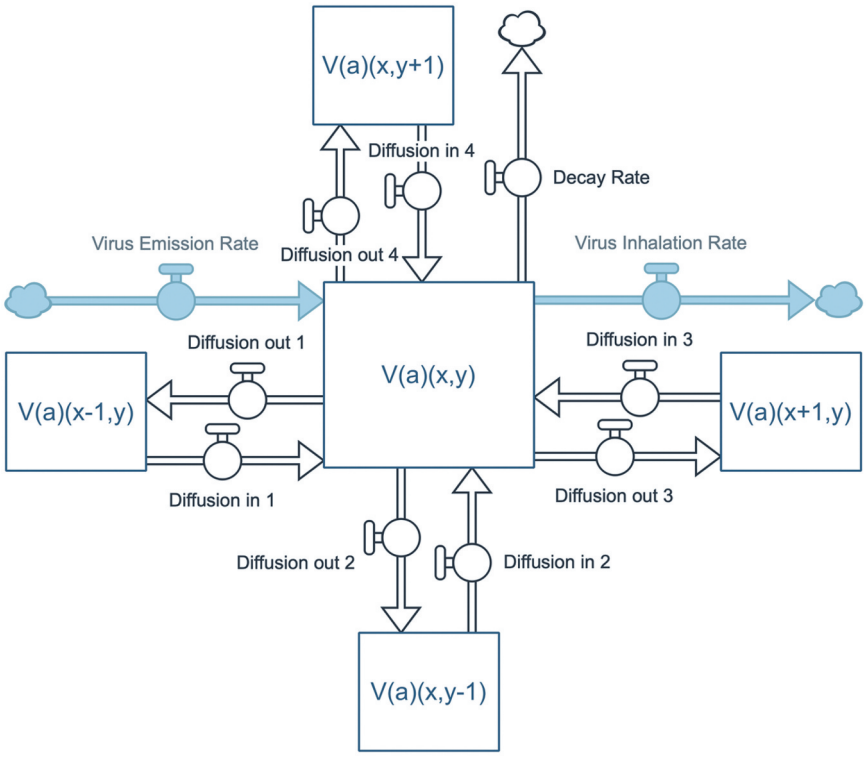

Figure 4. States, inflows, and outflows for the example of aerosol-induced virus contamination in grid cell (x, y), $V_{\text{aerosols}}\ (x, y)$, in the air layer (shown as $V(a)(x, y)$) (agent-triggered flows are shown as color-filled, whereas the environment-related flows have no fill color.)

The primary input to the expected economic activity is assumed to be the time spent by each guest in a venue. We assume that the expected payment of each guest $g \in E(pay)_g$, is an increasing function of their visiting time (Figure 5). The time spent by each guest in the venue is calculated from the agent-based script showing the entrance and leave time of each agent. Then, the expected revenue, $E(rev)$, is the sum of the expected payment collected from each agent.

$$E(rev) = \sum_{g=1}^{g=G} E(pay)_g \tag{3}$$

Acknowledging that the revenue functions would vary from one venue to another, our framework is flexible to allow any revenue function based on decision makers' preferences. Here, we use an illustrative function for the expected payment per guest (Figure 5) to demonstrate the operationalization of the model.

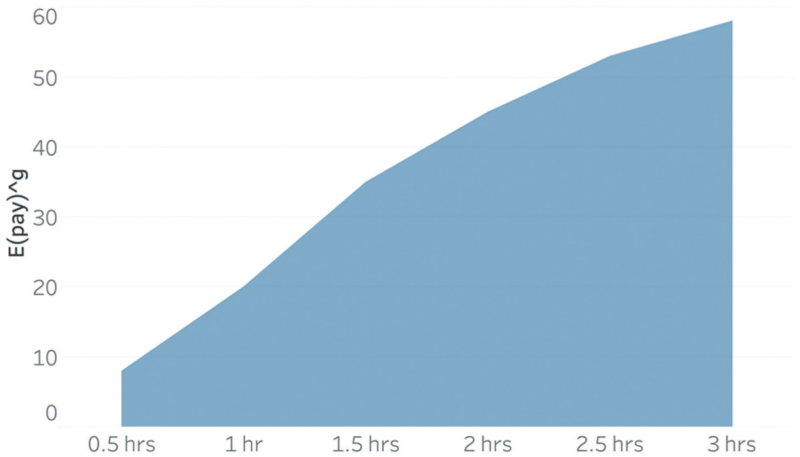

Figure 5. Illustrative function for the expected payment per guest based on visit duration.

Even though it is illustrative, the shape and parameters of the function in Figure 5 are chosen to be appropriate to the context, where (i) it is a piecewise linear function that initially has an increasing and then a decreasing slope, aiming to mimic the relationship between time spent by the customer and the courses ordered in a restaurant (e.g., starting with a snack or starter, then ordering one or two main courses, then a dessert, a drink etc.), and (ii) the output values of the function are in line with the recent statistics in the European setting (i.e., the Netherlands for our case), where an inexpensive meal per person starts from €10 and goes up to €60 in a mid-range restaurant (Numbeo, accessed May 31, 2025). This is consistent with our expected payment per guest function in Figure 5 where a person is expected to pay €8 for a 0.5-hour visit and €58 for a 3-hour visit.

2.2.4. Multi-criteria decision-making

In our hybrid model framework, we identify the best set of alternatives for operational decisions with multi-criteria decision-making. The best set of alternatives is defined as the set of non-dominated feasible options, and the goal is to provide the non-dominated set to the decision makers. As explained above, for each setting and scenario, the results of the expected R_{event} and $E(rev)$ are obtained and serve as objective functions, where the objectives are to minimize the expected R_{event} and maximize $E(rev)$. For each of these two objective function values, there are constraints that define their feasible regions:

- For the expected R_{event}, we assume that decision makers define a static risk threshold for the expected number of secondary infections per day/event, and the service options above that threshold are not acceptable,
- For the venue to run in an economically sustainable way, there is a minimum required revenue to be obtained per day. So, only the service options that have $E(rev)$ above the minimum required revenue are accepted as feasible.

Considering the two objective functions and their feasible regions, we define the Pareto frontier of non-dominated options as follows:

A solution X is said to dominate the other solution Y, if both the following conditions are true:

(1) The solution X is no worse than Y in both the expected R_{event} and $E(rev)$.
(2) The solution X is strictly better than Y in at least one objective, either the expected R_{event} or $E(rev)$.

For a given set of options, a pairwise comparison is made using the above definition and whether one point dominates the other is established. All points which are not dominated by any other member of the set are called the non-dominated options (Deb, 2011).

3. Results

The use of our hybrid model framework is demonstrated with an application for a restaurant case. We investigated the impact of four sets of operational decisions on the expected revenue and the risk of infection in an indoor restaurant setting: redesign of physical space (Section 3.1), average service duration (Section 3.2), service capacity (i.e., number of guests served in one day) (Section 3.3), and service scheme (i.e., combinations of (i) average service duration, (ii) service capacity, and (iii) the number of shifts) (Section 3.4).

Additionally, we investigated the impact of the following uncontrollable factors: (i) the infectious agent being a guest or service personnel (Section 3.1) and (ii) the infection prevalence within the community (Section 3.4 and 3.5).

The simulation experiment settings and the assumptions for the restaurant case study are:

- Seating capacity of 48 people, corresponding to 12 tables with 4 chairs each (Figure 6(a) for the Base layout).
- Fixed opening and closing hours, corresponding to 4 hours a day.
- All guests are scheduled to arrive at specific time slots, as would happen when using reservations.
- The restaurant can serve for one shift or multiple shifts a day, which is explicitly stated in relevant experiment settings.
- *The number of servings to tables by the staff* is proportional to the average service duration (i.e., a service staff visits a table every 30 minutes on average).
- Considering the time required for staff activities for each table and guest group, *the number of service staff* is proportional to the number of guests in a shift. (i.e., 2 service staff for 24 guests, 3 service staff for 36 guests, 4 service staff for 48 guests).
- Unless otherwise stated, it is assumed that a single guest is infectious during each experiment.
- In each simulation experiment, we generated 120 replications (5 for mobility behavior × 24 for the assignment of the infectious agent), which was calculated to correspond to an average relative error of 5% in mean infection risk and expected revenue at 95% confidence level (Law, 2007).

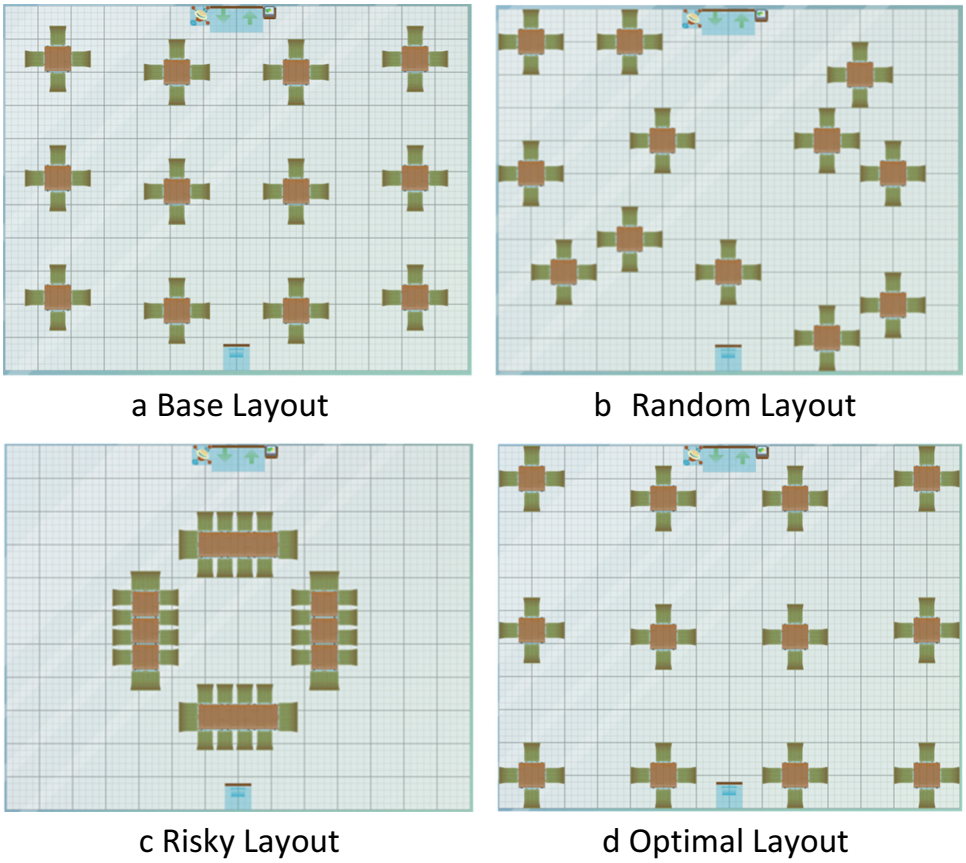

Figure 6. (a) Base Layout. (b) Random Layout. (c) Risky Layout. (d) Optimal Layout.

3.1. Impact of redesign of physical space

Redesigning the physical space by rearranging the distance between seating groups is one of the non-pharmaceutical interventions implemented during the recent COVID-19 pandemic, especially in the hospitality sector (CDC Center for Disease Control and Prevention, 2020; Wang et al., 2021; WHO World Health Organization, 2020). Rather than proposing the optimal layout for a particular restaurant, the aim of the simulation experiments in this section is to present a comparative analysis for the impact of different extreme layout settings on the infection risk. In these simulation experiments, we used a fixed service scheme (one shift, average service duration of 2 hours, service capacity of 48 people) and investigated the impact of four distinct layout settings:

- Base Layout: A setting with arbitrarily placed tables, in which the distance between two proximate chairs in different seating groups are at least 1.5 meters (Figure 6(a)).
- Random Layout: Tables are randomly placed using a random number generator, taking into account that the location of each table and its chairs do not overlap within the available space (Figure 6(b)).
- Risky Layout: This can be considered as the worst-case setting (from an epidemiological point of view), in which the tables are positioned close to each other as one large group, imitating a group event (Figure 6(c)).
- Optimal Layout: This can be considered as the best-case setting for the given number of tables and chairs and the dimensions of available space (Figure 6(d)). To find the optimal layout, we solved the optimization problem of *maximizing the minimum distance between any two tables* (Bortolete et al., 2022; Fischetti et al., 2021; Ugail et al., 2021). The model follows a similar structure to the "circle packing" problem presented in Bortolete et al. (2022), where one table and four chairs around it define the size of the circle. The model is solved on the discretized space and constraints the locations of tables and chairs (i) to be within the space, (ii) not to overlap with each other, (iii) not to overlap with the infrastructural elements in the venue, (iv) to be integers representing the grid cells. It should be noted that, here there are only a few infrastructural elements and a simple layout to demonstrate the impact of layout settings on the

infection risk; but for a case where other decorations, furniture or obstacles are a part of the physical space, the circle packing problem can easily be reconfigured to accommodate these constraints.

In these experiments, we investigated the impact of four layout settings under two scenarios (i) the infectious agent is a guest, and (ii) the infectious agent is personnel (Figure 7), since the design of physical space can affect contact structures in different ways for guests and personnel.

Recall that R_{event} represents the expected, average number of secondary infections, given that one of the agents is infectious. In Figure 7, the risky layout indicates the highest number of secondary infections, whereas the optimal layout leads to the lowest. While optimizing the layout relative to the base case has a minor effect, the risky layout is associated with 2.7-times and 1.8-times higher transmission risk figures with respect to base case in Guest and Personnel scenarios, respectively. Overall, in these experiments, the number of secondary infections caused by guests is found to be 3.5 times higher on average than that of personnel. The main reason behind this difference is that R_{event} is based on the agents' behavior while *present in the service area*. In the simulation, personnel enter the service area only when a task is assigned to them: here, the average time that a guest spends within the service area is 120 minutes, whereas it is 32 minutes for one service personnel. Infections that may occur in the kitchen area or elsewhere are thus not considered here. The expected revenue values do not differ between settings and scenarios, as the number of guests and the average service time are the same in all experiments.

3.2. Impact of service duration and service capacity

Contact duration and occupation density in indoor spaces are associated with the SARS-CoV-2 transmission risk (Bazant & Bush, 2021; Koh et al., 2020; Miller et al., 2021; Tang et al., 2020). In these simulation experiments, we investigated the impact of average service duration and service capacity on the infection risk, the number of secondary infections, R_{event}, and the expected revenue, $E(rev)$, for the following settings (Figure 8):

- Base layout (Figure 6(a))
- Average service duration: 0.5 - 3 hours, with 0.5 hours increments
- Service capacity: 24, 36, 48 people
- Two scenarios: (i) all guests enter the venue at the same time slot (like a scheduled event) (Figure 8), (ii) guests in different groups (i.e., different tables) enter the venue distributed over time slots (Table 1)

The simulation experiments in scenario (i) show that the number of secondary infections increases as the number of guests increases, but only when the service duration is longer than 1.5 hours (Figure 8). Additionally, the increasing impact of service duration on R_{event} is more evident than the impact of the number of guests. *This observation is due to a "circle of influence" around the infectious individual, which has a similar extent irrespective of the total number of guests but does enlarge with the visit duration*: Recall that R_{event} is the sum of the infection risk of all susceptible agents. Here, we define $w_{event}(inside)$ as "the

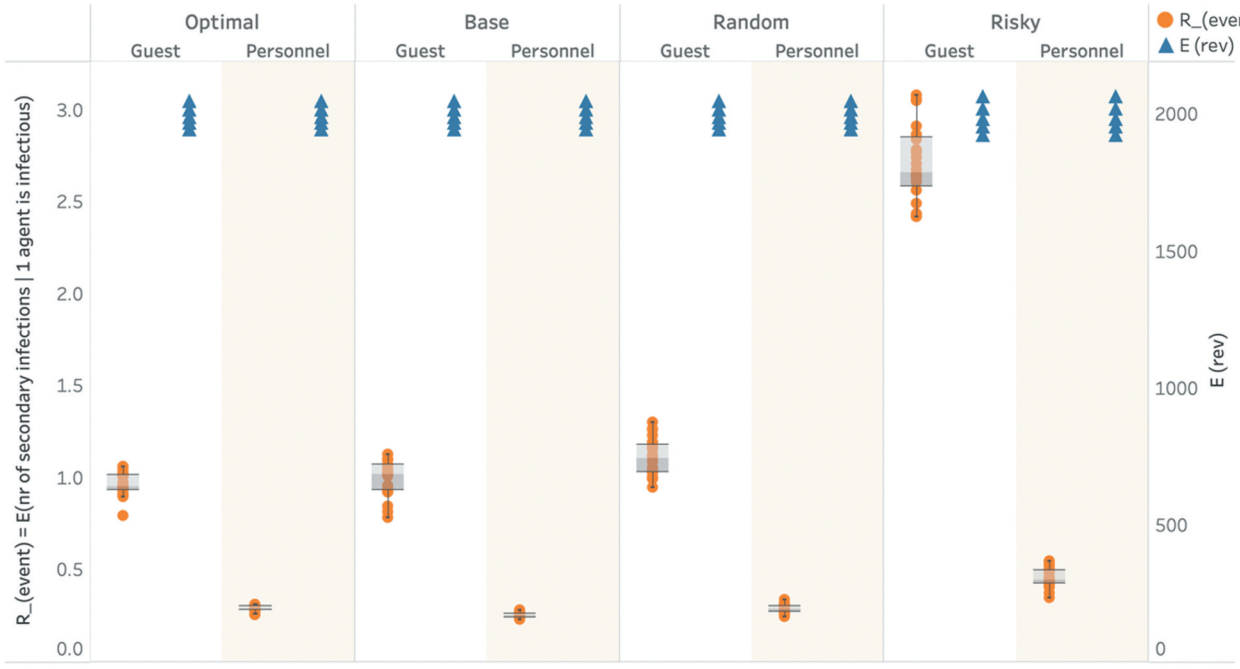

Figure 7. R_{event} and $E(rev)$ outcomes for different layout settings.

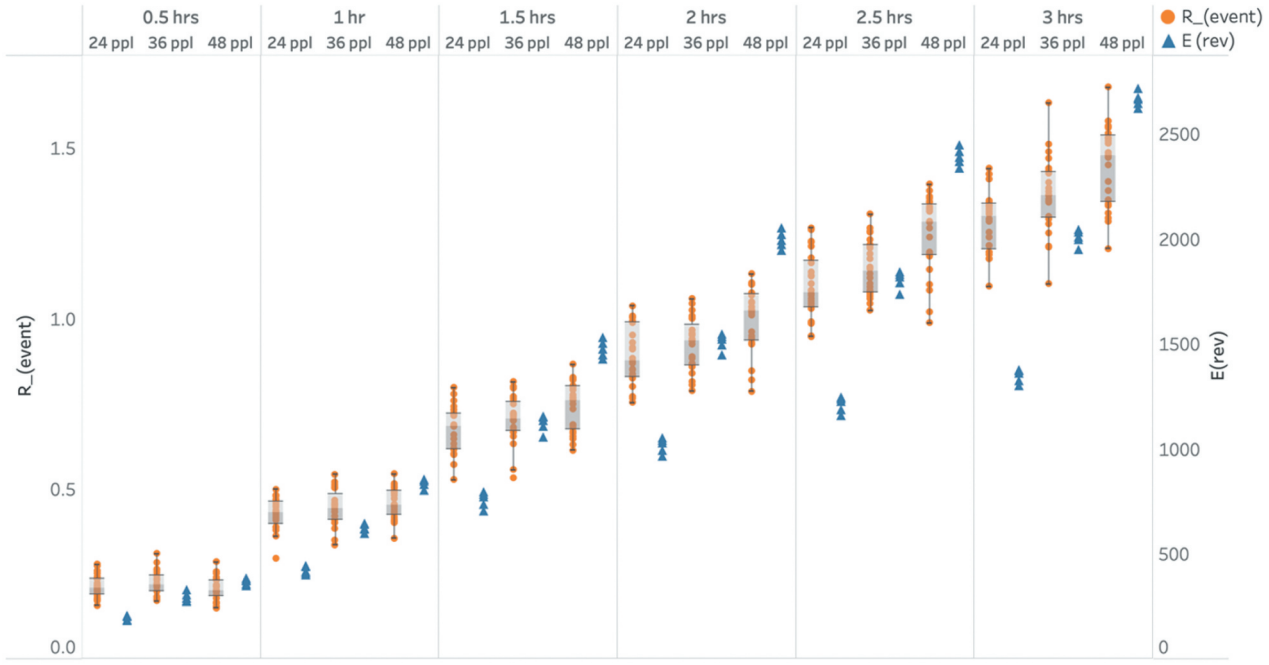

Figure 8. R_{event} and $E(rev)$ outcomes for changing service duration and service capacity levels in scenario (i) guests enter the venue at the same time slot.

percentage of R_{event} covering the susceptible agents sitting within 1.5-meters of the infectious individual". In these experiments, the average of $w_{event}(inside)$ is found to be between 75%-89% under different settings. That is, *the major portion of the risk stays within the social group of the infectious agent, and the influence of the number of visitors turns out to be limited.*

The average revenue increases in both the service capacity and the service duration. As the service time increases, the contribution of service capacity becomes more evident, since the expected revenue is defined as an increasing function of the service time.

Changing the entrance behavior from (i) entrance at the same time slot to (ii) entrance distributed over time slots shows a consistent but small contribution (Table 1): in all the experiment settings, R_{event} is smaller in the distributed scenario (4.7% on average, range of 0.5%–12.4%). R_{event} decreasing in (ii) can be explained by the reduced overlapping visiting time of the guests due to the definition of the scenario. The difference being limited between (i) and (ii) is also related to the *circle of influence*: by definition, guests sharing the same table enter the restaurant at around the same time, and the major portion of the risk is still within 1.5-meters of the infectious individual. Consequently, the contribution of scenario (ii) in mitigating the infection risk is found to be limited.

The revenue does not exhibit a difference between these two scenarios since scenarios do not have an impact on service duration and service capacity.

3.3. Impact of service schemes

A service scheme is identified as a combination of (i) average service duration, (ii) service capacity, and (iii) number of shifts in a day. Considering (i) and (iii) simultaneously constraints the solution space based on working hours: e.g., if the venue is open for 4 hours,

Table 1. R_{event} in (i) entrance at the same time slot and (ii) entrance distributed over time slots scenarios, and the percent decrease in R_{event} from (i) to (ii).

	0.5 hrs			1 hr			1.5 hrs		
	24 ppl	36 ppl	48 ppl	24 ppl	36 ppl	48 ppl	24 ppl	36 ppl	48 ppl
R_{event} in (i)	0.21	0.22	0.20	0.42	0.44	0.46	0.67	0.70	0.74
R_{event} in (ii)	0.20	0.21	0.19	0.41	0.41	0.41	0.64	0.64	0.66
% decrease	3.7%	6.5%	7.8%	4.3%	6.5%	8.0%	4.6%	8.4%	10.8%
	2 hrs			2.5 hrs			3 hrs		
	24 ppl	36 ppl	48 ppl	24 ppl	36 ppl	48 ppl	24 ppl	36 ppl	48 ppl
R_{event} in (i)	0.89	0.92	1.00	1.09	1.15	1.25	1.28	1.36	1.45
R_{event} in (ii)	0.87	0.92	0.87	1.07	1.10	1.17	1.26	1.34	1.41
% decrease	2.2%	0.5%	12.4%	1.8%	4.4%	5.8%	1.8%	1.8%	3.1%

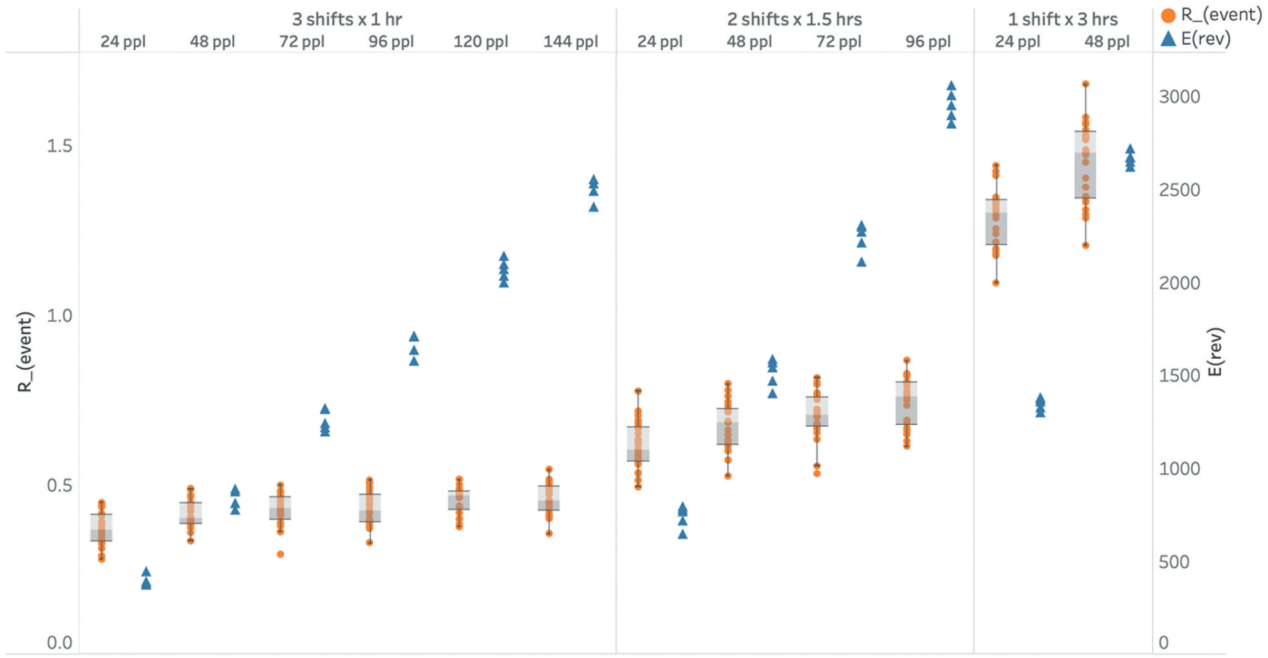

Figure 9. R_{event} and $E(rev)$ outcomes for different service schemes.

serving in 3 shifts with an average service duration of 1.5 would not be an option.

We selected a set of feasible service scheme options for the following experiments and investigated their impact on the expected number of infections and the expected revenue (Figure 9):

- Combinations of service durations and the number of shifts: 3 shifts of 1-hour duration, 2 shifts of 1.5 hours duration, 1 shift of 3 hours duration (assuming the restaurant still runs 4 hours in total but with short breaks between the shifts).
- Service capacity: Changing from 24 to 144 people (note that the service capacity is the total number of visitors accepted as the summation of all shifts in a day. For example, 144 people in the 3-shift case indicates 144/3 = 48 people are accepted during each shift).

Resonating with the previous experiments (Figure 8), the number of guests does not significantly impact the risk when the service duration in each shift is shorter (i.e., 1 hour) (Figure 9). However, as the duration gets longer, the circle of influence starts growing: on average, $w_{event}(outside)$ increases from 13% (in 1-hour shifts) to 20% (in 3-hour shifts), where $w_{event}(outside)$ is $1 - w_{event}(inside)$. Consequently, for longer service durations, R_{event} increases with the increasing number of guests. As the revenue function implies, expected revenue exhibits an increasing trend with the number of guests (Figure 9). Due to the piecewise linear structure of the expected payment function, the contribution of one unit of service capacity differs in each service scheme option. The highest expected revenue is generated in 2 shifts × 1.5-hour option, with a full service capacity of 48 people in each shift (48 × 2 = 96 people in total).

From the operational point of view, one of the key questions would be: "Are there any service schemes that perform better than the others in terms of both the infection risk and the expected economic activity?". To interpret this question, we compare the average performance of these schemes based on our two criteria: R_{event} and $E(rev)$ (Figure 10).

In these two criteria, the set of non-dominated (ND) solutions (i.e., a solution where none of the two criteria can be improved in value without degrading the other) are particularly shown with larger symbols and indicated by the ND mark and the resulting R_{event} values. By definition, all ND service options either have a lower risk or a higher revenue result compared to other options. One observation here is that the ND solution set consists of every 3-shift × 1-hour setting as well as a single 2-shift × 1.5-hours setting with a service capacity of 96 people. It should be noted that the identified ND solutions are not global but specific to the set of predefined service scheme options.

3.4. How to operate the venue: Identifying the Pareto frontier for the best set of service options

Up to now, we have investigated the impact of operational decisions on the infection risk and expected revenue, given that the condition of one of the agents is infectious. However, when the prevalence of the

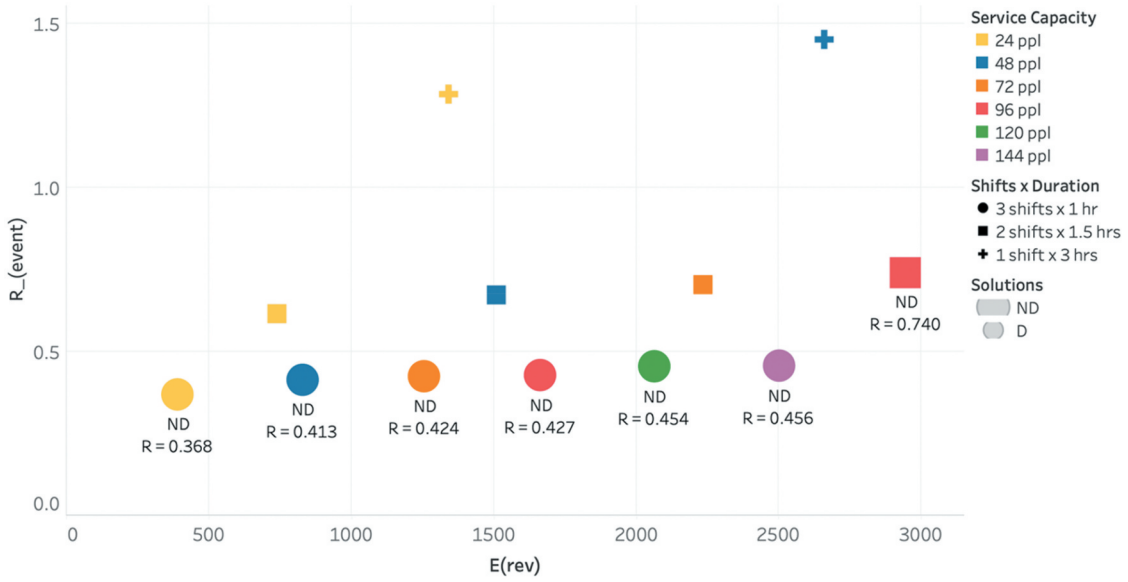

Figure 10. Average R_{event} and $E(rev)$ outcomes for different service schemes, highlighting ND service options.

infection in a community is considered, a more extensive service capacity with more visitors implies a higher chance of infectious introductions to the venue. Therefore, we incorporated the "probability of an agent in the event being infectious", $p-in_{event}$, into the calculations to obtain the expected number of secondary infections in the event.

$p-in_{event}$ is tightly connected to the term *infection prevalence*, $p-in$, which is the proportion of infectious individuals in the community at a time. In our experiments, we calculated $p-in_{event}$ as a function of $p-in$, indicating "the proportion of infectious individuals who do not have severe symptoms so that they can show up in a social space". In our example, $p-in_{event}$ is taken as 1.5% (prevalence of COVID-19 infections in January 2022) (Buitrago-Garcia et al., 2020; CBS Netherlands, 2022; RIVM Rijksinstituut voor Volksgezondheid en Milieu, 2022) (calculations are available in Appendix H). Then, along with the expected revenue, the expected infection risk (i.e., the expected number of secondary infections) for each service scheme is calculated as follows (Figure 11):

$$E(\text{infection risk})_{event} = E(\#\text{ of secondary infections})_{event} = R_{event} \times p-in_{event} \times \text{service capacity} \quad (4)$$

As mentioned previously, we assume that there is a *Minimum Required Revenue* for this social venue to continue its operations sustainably. Similarly, we assume that there is a risk threshold, *Maximum Risk*, that the decision makers consider as the upper limit for the expected number of secondary infections

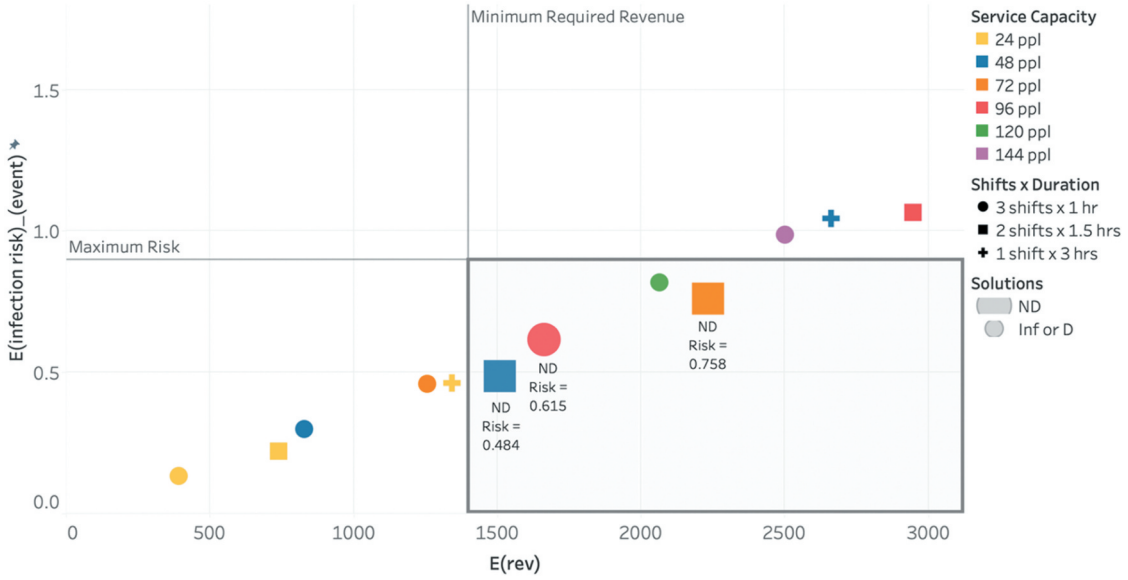

Figure 11. $E(\text{infection risk})_{event}$ and $E(rev)$ outcomes for different service schemes, highlighting ND service options.

(Figure 11). The shaded, lower right part of the solution set constitutes the feasible region for acceptable service options, below the risk threshold and above the required minimum revenue. Among the feasible service options, ND solutions constitute the Pareto-optimal solutions, i.e., the Pareto frontier, which are highlighted with larger-sized points.

After the feasibility conditions and $p - in_{event}$ are incorporated into the decisions, the set of ND solutions has changed (Figure 11). Compared to Figure 10, ND set size decreased to three, where most of the 3 shifts × 1-hour options are left out and new 2 shifts × 1.5-hours options are included. This response is because the expected infection risk depends on the number of guests, and a larger group of service scheme solutions were excluded because they are outside the feasible solution space.

3.5. The impact of infection prevalence in the population

In this section, we investigate the impact of infection prevalence values on the feasible service scheme options. As outlined above, the infection prevalence in the population is a dynamic variable that can take different values throughout a pandemic. Since it directly affects the probability of an infectious guest in a venue, the feasible set of service schemes changes with the infection prevalence. To demonstrate its impact, we calculated the performance of service schemes for two different infection prevalence values: a lower and higher $p - in_{event}$ with −50% and + 50% change to its base value of 1.5%, respectively (Figure 12).

When the prevalence is low (Figure 12(a)), the set of feasible solutions enlarges, and the size of ND service options increases to six. In that case, the decision maker has a larger *window of opportunity* to select among the best service schemes for their business. On the other hand, the number of feasible options decreases to one when the prevalence rises (Figure 12 (b)), and the *window of opportunity* starts to close. For even larger prevalence values, there would eventually be no feasible solution anymore, i.e., it would be either too risky or too costly to run the venue.

4. Discussion

In this study, we (i) investigated the impact of operational decisions on the transmission risk of a respiratory pathogen and the expected economic activity in indoor venues and (ii) illustrated how to identify the best set of service options to run the business both safely and sustainably for the case of SARS-CoV-2. To achieve this, we built a hybrid modeling and simulation framework incorporating human activity and virus spread in indoor venues with multi-criteria decision-making. We performed simulation experiments featuring a restaurant and examined the impact of different service decisions. The results illustrate that while some seating arrangements can substantially increase the infection risk, the mitigating impact of optimizing the layout can be limited. Service duration and service capacity are determinants of the expected economic activity, but they constitute a significant trade-off for the infection risk: the service duration has a substantial impact on the infection risk, and the service capacity drives the probability of infectious

a Lower Infection Prevalence Case
$p - in_{event}$ = 0.75%

b Higher Infection Prevalence Case
$p - in_{event}$ = 2.25%

Figure 12. (a) Lower infection prevalence case $p - in_{event}$ = 0.75%. (b) Higher infection prevalence case $p - in_{event}$ = 2.25%.

introductions. The analysis shows that the best service options critically depend on the infection prevalence in the community, highlighting that the epidemiological context should be considered in decision-making at the individual venue scale. For a given revenue function, our framework can support decision makers in identifying the best service options to run the venue both safely and sustainably.

Simulation modeling studies have been utilized to address various decision-making challenges in disease outbreak management and pandemic preparedness (Currie et al., 2020; Singh & Mathirajan, 2023). Among these challenges, operational decision-making at individual venues is crucial, given that contact and transmission between individuals primarily occur in these spaces, particularly indoors, which are associated with higher infection risks for respiratory pathogens. However, the impact of interventions is not clear at the individual venue scale due to the diverse characteristics of these spaces and the activities therein. We contribute to the existing literature with a hybrid model incorporating (i) pedestrian behavior and mobility, (ii) virus transmission dynamics in indoor spaces, and (iii) multi-criteria decision-making considering the economic indicators. Different from the multi-criteria approaches used in investigating SARS-CoV-2 mitigation strategies at the population level (Chandak et al., 2020; Chen et al., 2023; Colas et al., 2021; Gillis et al., 2021), we focused on identifying the best set of operational decisions that can be taken at an individual space.

In our simulation experiments, we evaluated the service decisions based on the infection risk and expected economic benefit for a given revenue function. With the assumption of a single infectious introduction, we found that the service schemes with the shortest service duration and the highest number of shifts constitute the major portion of the non-dominated solution set. Again, in that case, we found that (i) the service capacity drives the revenue substantially but not the infection risk caused by a single infected individual, (ii) the service duration has a more substantial impact on this infection risk when compared to the impact of service capacity, (iii) the contribution of scheduling the entrance of guests distributed over time slots instead of letting them enter the space around the same time is small. These findings are related to the *circle of influence* around the infectious person, i.e., the perimeter around an infectious person within which they can expose others to the virus. This circle enlarges with the visit duration because of the build-up of aerosolized virus particles in the environment. Contrarily, this perimeter is not affected by the service capacity, nor are there, in this setting, more guests within the perimeter. However, increasing the service capacity does result in more infectious introductions. Accordingly, instead of a single infectious agent, we incorporated the probability of infectious introductions to an event and calculated the expected infection risk. When incorporating the probability of infectious introductions, we find that the service capacity creates a considerable trade-off between the expected infection risk and revenue. Yet, this relationship crucially depends on the infection prevalence in the community. Overall, the level of infection prevalence defines our feasible and non-dominated solution set for the best service options. For the fixed level of service capacity, we also analyzed the impact of distinct behavioral patterns of individuals: infectious agent being a guest or personnel. The shorter duration of contacts elicited by personnel corresponds to substantially lower risks of successful virus transmission, highlighting the importance of accounting for the duration of individual contacts when assessing infection risks in a space. However, it should be noted that the infection risk in the model is based on the interactions in the service area, and infections related to personnel that may occur in the kitchen area or elsewhere are not considered in the results. Finally, while optimizing the physical rearrangement of the service area is often looked at for reducing infection risks, we find limited additional benefit in this specific setting while trying to keep the overall capacity (i.e., the total number of seats and tables) unaffected.

The generalizability of these results is subject to certain limitations, and future research would deliver additional research and practical implications. The model requires detailed parametrization related to biological processes (e.g., virus emission, environmental decay, diffusion rate, etc.) of the respiratory pathogen in question. Even for the special case of SARS-CoV-2, many parameters related to characterizations of the virus are still inconclusive in literature, are hard to measure empirically, or vary by setting or virus variant. With a series of sensitivity analyses, model results are shown to be robust to some level of uncertainty (Atamer Balkan et al., 2024). Even though a formal calibration could not be conducted due to a lack of reference data sets, the infection risk parameters (i.e., dose–response curve parameters) were chosen such that the distribution of outbreak sizes was in line with epidemiological observations from similar social settings during the initial stages of the COVID-19 pandemic (Adam et al., 2020). The model parameters will be updated as new evidence becomes available in the field. The scope of this paper is indoor venues of a particular service sector, such as restaurants, bars, and cafes. In ongoing research, the framework is being applied to other social environments, such as retail and educational settings. Despite these limitations, general findings on the positive relation between time expenditure and the perimeter at which infections can take place, are expected to be generalizable across a range of settings, particularly those

where agents are relatively stationary (e.g., theatre/auditorium, classrooms, office spaces).

Owing to the modular setup of PeDViS, it can be used to characterize the infection risks in other types of indoor spaces, and the model can be adapted to different SARS-CoV-2 variants and other respiratory pathogens, as explained in Appendix I. PeDViS can also support decision-making for the mitigation strategies considering other non-pharmaceutical interventions, such as the use of masks and ventilation (Atamer Balkan et al., 2024). In future research, the model will be configured to different types of individual heterogeneities, including infectiousness, vaccination status, and test result. In doing so, we will be able to incorporate various vaccination- and/or test-based entry restriction policies into the model.

This study contributes to our understanding of the impact of operational decisions in indoor venues on the respiratory pathogen transmission risk and the expected economic activity. Our hybrid framework combines behavioral and epidemiological models with economic indicators constituting a considerable example of interdisciplinary hybrid modeling study. With the help of the modular nature of these models, the framework can readily be extended to different settings, activities, and revenue functions and can be applied to different respiratory pathogens. In all, the hybrid framework can help policymakers and social venue partners make informed decisions to run indoor social spaces safely and sustainably.

Acknowledgments

We thank Colin Teberg, You Chang, and Bas Dado for their support in both research and software development.

Disclosure statement

No potential conflict of interest was reported by the author(s).

Funding

This work was supported by the Dutch Research Council (NWO) and ZonMw as a part of the project SamenSlimOpen (with project number 10430022010018) of the research program COVID-19 Programma.

Data availability statement

The PeDViS model software at the core of the framework is developed in Python, and the multi-criteria decision analysis is conducted in R. All the code for the PeDViS model, data to reproduce the described simulation experiments, and the R code used for multi-criteria decision analysis are openly available on Gitlab (https://git.wur.nl/sso-public/pedvis-simulator). An open-access web-based simulation environment is also available through the SamenSlimOpen App website (https://www.samenslimopen.nl/de-tool/).

References

Adam, D. C., Wu, P., Wong, J. Y., Lau, E. H., Tsang, T. K., Cauchemez, S., Leung, G. M., & Cowling, B. J. (2020). Clustering and superspreading potential of SARS-CoV-2 infections in Hong Kong. *Nature Medicine*, *26*(11), 1714–1719. https://doi.org/10.1038/s41591-020-1092-0

Alım, M., & Kesen, S. E. (2023). Investigating the effects of various control measures on economy and spread of COVID-19 in Turkey: A system dynamics approach. *Simulation*, *99*(2), 113–125. https://doi.org/10.1177/00375497221116641

Angelopoulou, A., & Mykoniatis, K. (2024). Hybrid modelling and simulation of the effect of vaccination on the COVID-19 transmission. *Journal of Simulation*, *18*(1), 88–99. https://doi.org/10.1080/17477778.2022.2062260

Araz, O. M. (2013). Integrating complex system dynamics of pandemic influenza with a multi-criteria decision making model for evaluating public health strategies. *Journal of Systems Science and Systems Engineering*, *22*(3), 319–339. https://doi.org/10.1007/s11518-013-5220-y

Araz, O. M., Lant, T., Fowler, J. W., & Jehn, M. (2011). A simulation model for policy decision analysis: A case of pandemic influenza on a university campus. *Journal of Simulation*, *5*(2), 89–100. https://doi.org/10.1057/jos.2010.6

Atamer Balkan, B., Chang, Y., Sparnaaij, M., Wouda, B., Boschma, D., Liu, Y., Yuan, Y., Daamen, W., de Jong, M. C. M., Teberg, C., Schachtschneider, K., Sikkema, R. S., van Veen, L., Duives, D., & ten Bosch, Q. A. (2024). The multi-dimensional challenges of controlling respiratory virus transmission in indoor spaces: Insights from the linkage of a microscopic pedestrian simulation and SARS-CoV-2 transmission model. *PLOS Computational Biology*, *20*(3), e1011956. https://doi.org/10.1371/journal.pcbi.1011956

Bazant, M. Z., & Bush, J. W. (2021). A guideline to limit indoor airborne transmission of COVID-19. *Proceedings of the National Academy of Sciences*, *118*(17). https://doi.org/10.1073/pnas.2018995118

Barlas, Y. (1996). Formal aspects of model validity and validation in system dynamics. System Dynamics Review: The Journal of the System Dynamics Society, 12 (3), 183-210.

Bortolete, J. C., Bueno, L. F., Butkeraites, R., Chaves, A. A., Collaço, G., Magueta, M., Pelogia, F. J. R., Neto, L. L. S., Santos, T. S., Silva, T. S., Sobral, F. N. C., & Yanasse, H. H. (2022). A support tool for planning classrooms considering social distancing between students. *Computational & Applied Mathematics*, *41*(1), 1–23. https://doi.org/10.1007/s40314-021-01718-w

Brailsford, S. C., Eldabi, T., Kunc, M., Mustafee, N., & Osorio, A. F. (2019). Hybrid simulation modelling in operational research: A state-of-the-art review. *European Journal of Operational Research*, *278*(3), 721–737. https://doi.org/10.1016/j.ejor.2018.10.025

Brizek, M. G., Frash, R. E., McLeod, B. M., & Patience, M. O. (2021). Independent restaurant operator perspectives in the wake of the COVID-19 pandemic. *International Journal of Hospitality Management*, *93*, 102766. https://doi.org/10.1016/j.ijhm.2020.102766

Buitrago-Garcia, D., Egli-Gany, D., Counotte, M. J., Hossmann, S., Imeri, H., Ipekci, A. M., Salanti, G., & Low, N. (2020). Occurrence and transmission potential of asymptomatic and presymptomatic SARS-CoV-2 infections: A living systematic review and meta-analysis.

PLOS Medicine, *17*(9), e1003346. https://doi.org/10.1371/journal.pmed.1003346

Bulfone, T. C., Malekinejad, M., Rutherford, G. W., & Razani, N. (2021). Outdoor transmission of SARS-CoV-2 and other respiratory viruses: A systematic review. *The Journal of Infectious Diseases*, *223*(4), 550–561. https://doi.org/10.1093/infdis/jiaa742

Callaway, E. (2020). Dozens to be deliberately infected with coronavirus in UK 'human challenge' trials. Nature, 586 (7831), 651-653.

Campanella, M. C., Hoogendoorn, S., & Daamen, W. (2014). Quantitative and qualitative validation procedure for general use of pedestrian models. In U. Weidmann, U. Kirsch, & M. Schreckenberg (Eds.), Pedestrian and Evacuation Dynamics 2012 (pp. 891–905). Springer International Publishing.

Campanella, M. C., Hoogendoorn, S. P., & Daamen, W (2009). Improving the Nomad microscopic walker model. IFAC Proceedings Volumes, 42, 12–18.

Campanella, M. C. (2016). *Microscopic modelling of walking behaviour* [Doctoral dissertation]. Delft University of Technology.

CBS (Centraal Bureau voor de Statistiek) Netherlands. (2022, May). *Bevolkingsontwikkeling; regio per maand (Population development; region per month)*. https://opendata.cbs.nl/statline/#/CBS/nl/dataset/37230ned/table)

CDC (Center for Disease Control and Prevention). (2020). *Considerations for restaurants and bars (by National Center for Immunization and Respiratory Diseases (US). Division of Viral Diseases). Coronavirus disease 2020 (COVID-19) series*. Retrieved May 18, 2020 from https://stacks.cdc.gov/view/cdc/88184

Chandak, A., Dey, D., Mukhoty, B., & Kar, P. (2020). Epidemiologically and socio-economically optimal policies via Bayesian optimization. *Transactions of the Indian National Academy of Engineering*, *5*(2), 117–127. https://doi.org/10.1007/s41403-020-00142-6

Chen, K., Pun, C. S., & Wong, H. Y. (2023). Efficient social distancing during the COVID-19 pandemic: Integrating economic and public health considerations. *European Journal of Operational Research*, *304*(1), 84–98. https://doi.org/10.1016/j.ejor.2021.11.012

Cheng, P., Luo, K., Xiao, S., Yang, H., Hang, J., Ou, C., Li, B. J., Yen, H.-L., Hui, D. S., Hu, S., & Li, Y. (2022). Predominant airborne transmission and insignificant fomite transmission of SARS-CoV-2 in a two-bus COVID-19 outbreak originating from the same pre-symptomatic index case. *Journal of Hazardous Materials*, *425*, 128051. https://doi.org/10.1016/j.jhazmat.2021.128051

Colas, C., Hejblum, B., Rouillon, S., Thiébaut, R., Oudeyer, P. Y., Moulin-Frier, C., & Prague, M. (2021). EpidemiOptim: A toolbox for the optimization of control policies in epidemiological models. *The Journal of Artificial Intelligence Research*, *71*, 479–519. https://doi.org/10.1613/jair.1.12588

Contardo, C., & Costa, L. (2022). On the optimal layout of a dining room in the era of COVID-19 using mathematical optimization. *International Transactions in Operational Research*, *29*(6), 3294–3315. https://doi.org/10.1111/itor.13139

Currie, C. S., Fowler, J. W., Kotiadis, K., Monks, T., Onggo, B. S., Robertson, D. A., & Tako, A. A. (2020). How simulation modelling can help reduce the impact of COVID-19. *Journal of Simulation*, *14*(2), 83–97. https://doi.org/10.1080/17477778.2020.1751570

Deb, K. (2011). Multi-objective optimisation using evolutionary algorithms: An introduction. In Wang, L., Ng, A. H. C, Deb, K. (Eds.), *Multi-objective evolutionary optimisation for product design and manufacturing* (pp. 3–34). Springer London. https://doi.org/10.1007/978-0-85729-652-8_1

Deijkers, E. (2022). Comparing various measures to prevent covid-19 spread in offices through simulation modelling (Master thesis, Delft University of Technology). http://resolver.tudelft.nl/uuid:6f11dc81-0260-4dd4-bb98-cd74275a3c42.

de Mooij, J., Bhattacharya, P., Dell'anna, D., Dastani, M., Logan, B., & Swarup, S. (2023). A framework for modeling human behavior in large-scale agent-based epidemic simulations. *Simulation*, *99*(12), 1183–1211. https://doi.org/10.1177/00375497231184898

Duggan, J., Andrade, J., Murphy, T. B., Gleeson, J. P., Walsh, C., & Nolan, P. (2024). An age-cohort simulation model for generating COVID-19 scenarios: A study from Ireland's pandemic response. *European Journal of Operational Research*, *313*(1), 343–358. https://doi.org/10.1016/j.ejor.2023.08.011

Dunke, F., & Nickel, S. (2021). Simulation-based multi-criteria decision making: An interactive method with a case study on infectious disease epidemics. *Annals of Operations Research*, 1–30. https://doi.org/10.1007/s10479-021-04321-8

Eryarsoy, E., Shahmanzari, M., & Tanrisever, F. (2023). Models for government intervention during a pandemic. *European Journal of Operational Research*, *304*(1), 69–83. https://doi.org/10.1016/j.ejor.2021.12.036

Filipe, L., de Almeida, S. V., Costa, E., da Costa, J. G., Lopes, F. V., Santos, J. V., & Morrissey, K. (2022). Trade-offs during the COVID-19 pandemic: A discrete choice experiment about policy preferences in Portugal. *PLOS ONE*, *17*(12), e0278526. https://doi.org/10.1371/journal.pone.0278526

Fischetti, M., Fischetti, M., & Stoustrup, J. (2021). Safe distancing in the time of COVID-19. *European Journal of Operational Research*, *304*(1), 139–149. https://doi.org/10.1016/j.ejor.2021.07.010

Fisher, K. A., Tenforde, M. W., Feldstein, L. R., Lindsell, C. J., Shapiro, N. I., Files, D. C., Gibbs, K. W., Erickson, H. L., Prekker, M. E., Steingrub, J. S., Exline, M. C., Henning, D. J., Wilson, J. G., Brown, S. M., Peltan, I. D., Rice, T. W., Hager, D. N., Ginde, A. A.Talbot, H. K., & IVY Network Investigators. (2020, July). Community and close contact exposures associated with COVID-19 among symptomatic adults≥18 years in 11 outpatient health care facilities-united states. *MMWR Morbidity and Mortality Weekly Report*, *69*(36), 1258. https://doi.org/10.15585/mmwr.mm6936a5

Gerhards, N. M., Gonzales, J. L., Vreman, S., Ravesloot, L., van den Brand, J. M., Doekes, H. P., de Jong, M. C., Stegeman, A., Oreshkova, N., van der Poel, W. H. M., & de Jong, M. C. M. (2023). Efficient direct and limited environmental transmission of SARS-CoV-2 lineage B. 1.22 in domestic cats. *Microbiology Spectrum*, *11*(3), e02553–22. https://doi.org/10.1128/spectrum.02553-22

Gillis, M., Urban, R., Saif, A., Kamal, N., & Murphy, M. (2021). A simulation-optimization framework for optimizing response strategies to epidemics. *Operations Research Perspectives*, *8*, 100210. https://doi.org/10.1016/j.orp.2021.100210

Greenhalgh, T., Jimenez, J. L., Prather, K. A., Tufekci, Z., Fisman, D., & Schooley, R. (2021). Ten scientific reasons in support of airborne transmission of SARS-CoV-2.

Lancet, *397*(10285), 1603–1605. https://doi.org/10.1016/S0140-6736(21)00869-2

Gursoy, D., & Chi, C. G. (2020). Effects of COVID-19 pandemic on hospitality industry: Review of the current situations and a research agenda. *Journal of Hospitality Marketing and Management*, *29*(5), 527–529. https://doi.org/10.1080/19368623.2020.1788231

Hutton, D. W. (2013). Review of operations research tools and techniques used for influenza pandemic planning. In G. Zaric (Ed.), *Operations research and health care policy. International series in operations research & management science* (Vol. 190, 225–247). New York, NY: Springer.

Islam, M. T., Jain, S., Chen, Y., Chowdhury, B. D. B., & Son, Y. J. (2021). An agent-based simulation model to evaluate contacts, layout, and policies in entrance, exit, and seating in indoor activities under a pandemic situation. *IEEE Transactions on Automation Science and Engineering*, *19*(2), 603–619.

Ivanov, D. (2020). Predicting the impacts of epidemic outbreaks on global supply chains: A simulation-based analysis on the coronavirus outbreak (COVID-19/SARS-CoV-2) case. *Transportation Research Part E: Logistics & Transportation Review*, *136*, 101922. https://doi.org/10.1016/j.tre.2020.101922

Kar, E., Fakhimi, M., Turner, C., & Eldabi, T. (2024). Hybrid simulation in healthcare: A systematic exploration of models, applications, and emerging trends. *Journal of Simulation*, *19*(2), 231–249. https://doi.org/10.1080/17477778.2024.2354250

Kerr, C. C., Stuart, R. M., Mistry, D., Abeysuriya, R. G., Rosenfeld, K., Hart, G. R., Klein, D. J., Cohen, J. A., Selvaraj, P., Hagedorn, B., George, L., Jastrzębski, M., Izzo, A. S., Fowler, G., Palmer, A., Delport, D., Scott, N., Kelly, S. L.Bennette, C. S. … & Famulare, M. (2021). Covasim: An agent-based model of COVID-19 dynamics and interventions. *PLOS Computational Biology*, *17*(7), e1009149. https://doi.org/10.1371/journal.pcbi.1009149

Koh, W. C., Naing, L., Chaw, L., Rosledzana, M. A., Alikhan, M. F., Jamaludin, S. A., Amin, F., Omar, A., Shazli, A., Griffith, M., Pastore, R., & Wong, J. (2020). What do we know about SARS-CoV-2 transmission? A systematic review and meta-analysis of the secondary attack rate and associated risk factors. *PLOS ONE*, *15*(10), e0240205. https://doi.org/10.1371/journal.pone.0240205

Law, A. M. (2007). *Simulation modeling and analysis* (4th ed.). McGraw-Hill.

Lee, B., Lee, M., Mogk, J., Goldstein, R., Bibliowicz, J., Brudy, F., & Tessier, A. (2021). Designing a multi-agent occupant simulation system to support facility planning and analysis for COVID-19. *Proceedings of the 2021 ACM Designing Interactive Systems Conference*, (pp. 15–30).

Lee, B. Y., Brown, S. T., Korch, G. W., Cooley, P. C., Zimmerman, R. K., Wheaton, W. D., Zimmer, S. M., Grefenstette, J. J., Bailey, R. R., Assi, T.-M., & Burke, D. S. (2010). A computer simulation of vaccine prioritization, allocation, and rationing during the 2009 H1N1 influenza pandemic. *Vaccine*, *28*(31), 4875–4879. https://doi.org/10.1016/j.vaccine.2010.05.002

Lewis, D. (2021). COVID-19 rarely spreads through surfaces. So why are we still deep cleaning? *Nature*, *590*(7844), 26–28. https://doi.org/10.1038/d41586-021-00251-4

Li, S., Xu, Y., Cai, J., Hu, D., & He, Q. (2021). Integrated environment-occupant-pathogen information modeling to assess and communicate room-level outbreak risks of infectious diseases. *Building & Environment*, *187*, 107394. https://doi.org/10.1016/j.buildenv.2020.107394

Martinez, I., Bruse, J. L., Florez-Tapia, A. M., Viles, E., & Olaizola, I. G. (2022). ArchABM: An agent-based simulator of human interaction with the built environment. CO2 and viral load analysis for indoor air quality. *Building & Environment*, *207*, 108495. https://doi.org/10.1016/j.buildenv.2021.108495

Miller, S. L., Nazaroff, W. W., Jimenez, J. L., Boerstra, A., Buonanno, G., Dancer, S. J., Kurnitski, J., Marr, L. C., Morawska, L., & Noakes, C. (2021). Transmission of SARS-CoV-2 by inhalation of respiratory aerosol in the Skagit Valley Chorale superspreading event. *Indoor Air*, *31*(2), 314–323. https://doi.org/10.1111/ina.12751

Moore, J. F., Carvalho, A., Davis, G. A., Abulhassan, Y., & Megahed, F. M. (2021). Seat assignments with physical distancing in single-destination public transit settings. *IEEE Access*, *9*, 42985–42993. https://doi.org/10.1109/ACCESS.2021.3065298

Müller, S. A., Balmer, M., Charlton, W., Ewert, R., Neumann, A., Rakow, C., Schlenther, T., & Nagel, K. (2021). Predicting the effects of COVID-19 related interventions in urban settings by combining activity-based modelling, agent-based simulation, and mobile phone data. *PLOS ONE*, *16*(10), e0259037. https://doi.org/10.1371/journal.pone.0259037

Mustafee, N., Tolk, A., Ramamohan, V., & Strassburger, S. (2025). Editorial: Hybrid modelling and simulation. *Journal of Simulation*, *19*(2), 125–126. https://doi.org/10.1080/17477778.2025.2468202

Nguyen, L. K., Howick, S., & Megiddo, I. (2024). A framework for conceptualising hybrid system dynamics and agent-based simulation models. *European Journal of Operational Research*, *315*(3), 1153–1166. https://doi.org/10.1016/j.ejor.2024.01.027

Nicas, M. (1996). An analytical framework for relating dose, risk, and incidence: An application to occupational tuberculosis infection. *Risk Analysis: An Official Publication of the Society for Risk Analysis*, *16*(4), 527–538. https://doi.org/10.1111/j.1539-6924.1996.tb01098.x

Norris, C. L., Taylor Jr, S., Jr., & Taylor, D. C. (2021). Pivot! How the restaurant industry adapted during COVID-19 restrictions. *International Hospitality Review*, *35*(2), 132–155. https://doi.org/10.1108/IHR-09-2020-0052

Ntounis, N., Mumford, C., Loroño-Leturiondo, M., Parker, C., & Still, K. (2020). How safe is it to shop? Estimating the amount of space needed to safely social distance in various retail environments. *Safety Science*, *132*, 104985. https://doi.org/10.1016/j.ssci.2020.104985

Numbeo. (2025). *Cost of living in Netherlands*. https://www.numbeo.com/cost-of-living/country_result.jsp?country=Netherlands

Panovska-Griffiths, J., Kerr, C. C., Waites, W., & Stuart, R. M. (2021). Mathematical modeling as a tool for policy decision making: Applications to the COVID-19 pandemic. In Arni, S.R., Rao, C.R (Eds.), *Handbook of statistics* (Vol. 44, pp. 291–326). Elsevier.

Popa, A., Genger, J. W., Nicholson, M. D., Penz, T., Schmid, D., Aberle, S. W., & Bergthaler, A. (2020). Genomic epidemiology of superspreading events in Austria reveals mutational dynamics and transmission properties of SARS-CoV-2. *Science Translational Medicine*, *12*(573), eabe2555.

RIVM (Rijksinstituut voor Volksgezondheid en Milieu). (2022, May). *RIVM coronavirus dashboard*. https://coronadashboard.government.nl/landelijk/positief-geteste-mensen

Silal, S. P. (2021). Operational research: A multidisciplinary approach for the management of infectious disease in a

global context. *European Journal of Operational Research*, *291*(3), 929–934. https://doi.org/10.1016/j.ejor.2020.07.037

Singh, R., & Mathirajan, M. (2023). Simulation modelling techniques for managing epidemic outbreak: A review, classification schemes, and meta-analysis. *Journal of Simulation*, *17*(6), 709–728. https://doi.org/10.1080/17477778.2022.2067012

Sparnaaij, M., Yuan, Y., Daamen, W., & Duives, D. C. (2024). Using pedestrian modelling to inform virus transmission mitigation policies: A novel activity scheduling model to enable virus transmission risk assessment in a restaurant environment. *Physica A: Statistical Mechanics and Its Applications*, *633*, 129395. https://doi.org/10.1016/j.physa.2023.129395

Tang, S., Mao, Y., Jones, R. M., Tan, Q., Ji, J. S., Li, N., Shen, J., Lv, Y., Pan, L., Ding, P., Wang, X., Wang, Y., MacIntyre, C. R., & Shi, X. (2020). Aerosol transmission of SARS-CoV-2? Evidence, prevention and control. *Environment International*, *144*, 106039. https://doi.org/10.1016/j.envint.2020.106039

Ugail, H., Aggarwal, R., Iglesias, A., Howard, N., Campuzano, A., Suárez, P., Maqsood, M., Aadil, F., Mehmood, I., Gleghorn, S., Taif, K., Kadry, S., & Muhammad, K. (2021). Social distancing enhanced automated optimal design of physical spaces in the wake of the COVID-19 pandemic. *Sustainable Cities and Society*, *68*, 102791. https://doi.org/10.1016/j.scs.2021.102791

Vázquez-Abad, F. J., Dufresne, D., & Park, G. B. (2022,). Impact of vaccination policies for COVID-19 using hybrid simulation. *2022 Winter Simulation Conference (WSC)* (pp. 545–556). IEEE. https://doi.org/10.1109/WSC57314.2022.10015370

Viana, J., Brailsford, S. C., Harindra, V., & Harper, P. R. (2014). Combining discrete-event simulation and system dynamics in a healthcare setting: A composite model for chlamydia infection. *European Journal of Operational Research*, *237*(1), 196–206. https://doi.org/10.1016/j.ejor.2014.02.052

Volpatto, D. T., Resende, A. C., Anjos, L., Silva, D., Dias, C. M., Almeida, R. C., & Malta, S. M. (2023). A generalised SEIRD model with implicit social distancing mechanism: A Bayesian approach for the identification of the spread of COVID-19 with applications in Brazil and Rio de Janeiro state. *Journal of Simulation*, *17*(2), 178–192. https://doi.org/10.1080/17477778.2021.1977731

Wang, D., Yao, J., & Martin, B. A. (2021). The effects of crowdedness and safety measures on restaurant patronage choices and perceptions in the COVID-19 pandemic. *International Journal of Hospitality Management*, *95*, 102910. https://doi.org/10.1016/j.ijhm.2021.102910

Watanabe, T., Bartrand, T. A., Weir, M. H., Omura, T., & Haas, C. N.. (2010). Development of a dose-response model for SARS coronavirus. Risk Analysis: An International Journal, 30(7), 1129-1138.

Wang, X. (2021). Quantifying transmission risks of SARS-CoV-2 in pedestrian interactions at large events (Master thesis, Delft University of Technology). http://resolver.tudelft.nl/uuid:2b4d3e48-28da-4e1f-bb21-0c828d99bd26 .

WHO (World Health Organization). (2020, August 25). *COVID-19 management in hotels and other entities of the accommodation sector: Interim guidance* (No. WHO/2019-nCoV/hotels/2020.3). World Health Organization.

Xiao, Y., Yang, M., Zhu, Z., Yang, H., Zhang, L., & Ghader, S. (2021). Modeling indoor-level non-pharmaceutical interventions during the COVID-19 pandemic: A pedestrian dynamics-based microscopic simulation approach. *Transport Policy*, *109*, 12–23. https://doi.org/10.1016/j.tranpol.2021.05.004

Ying, F., O'Clery, N., & Simuunza, M. C. (2021). Modelling COVID-19 transmission in supermarkets using an agent-based model. *PLOS ONE*, *16*(4), e0249821. https://doi.org/10.1371/journal.pone.0249821

Zhang, N., Chen, X., Jia, W., Jin, T., Xiao, S., Chen, W., Hang, J., Ou, C., Lei, H., Qian, H., Su, B., Li, J., Liu, D., Zhang, W., Xue, P., Liu, J., Weschler, L. B., Xie, J., Li, Y., & Kang, M. (2021). Evidence for lack of transmission by close contact and surface touch in a restaurant outbreak of COVID-19. *The Journal of Infection*, *83*(2), 207–216. https://doi.org/10.1016/j.jinf.2021.05.030

Zhang, R., Li, Y., Zhang, A. L., Wang, Y., & Molina, M. J. (2020). Identifying airborne transmission as the dominant route for the spread of COVID-19. *Proceedings of the National Academy of Sciences*, *117*(26), 14857–14863. https://doi.org/10.1073/pnas.2009637117

Zhou, Y., Nikolaev, A., Bian, L., Lin, L., & Li, L. (2021). Investigating transmission dynamics of influenza in a public indoor venue: An agent-based modeling approach. *Computers & Industrial Engineering*, *157*, 107327. https://doi.org/10.1016/j.cie.2021.107327

Zhu, H., Liu, S., Li, X., Zhang, W., Osgood, N., & Jia, P. (2025). Using a hybrid simulation model to assess the impacts of combined COVID-19 containment measures in a high-speed train station. *Journal of Simulation*, *19*(2), 141–165. https://doi.org/10.1080/17477778.2023.2189027

Appendices

Appendix A. Additional Assumptions of the Model

Queuing: In terms of activities and mobility, the queuing behavior of agents are not considered in this paper, even though the model framework is capable of incorporating it. Our project team conducted an empirical study to assess the nature of queuing behavior in small and middle-sized restaurants, and found out that the queues in the restaurants typically consist of no more than 2 people and the waiting time at the coat rack and pay register is within 20-50 seconds. Since such short duration contacts are not associated with significant infection risks (Ying & O'Clery, 2021), these short queues are not considered in this paper.

Mitigation tools: Regarding respiratory virus transmission, mitigation tools such as table dividers, sneeze guards and plastic barriers between tables can also be considered relevant objects, but they are not included in this particular paper since their use was not a typical intervention in the Netherlands during the recent COVID-19 pandemic.

Appendix B. Agent-Based Movement Model (NOMAD) Equations

The following set of equations governs the movement of each pedestrian in NOMAD:

$$\frac{d}{dt}\vec{p}_i(t) = \vec{v}_i(t) \tag{A1}$$

$$\frac{d}{dt}\vec{v}_i(t) = \vec{a}_i(t) \tag{A2}$$

$$\vec{a}_i(t) = \vec{a}_{f;i}(t) + \vec{a}_{o;i}(t) + \vec{a}_{a;i}(t) + \vec{\xi} \tag{A3}$$

$$\vec{a}_{f;i}(t) = \frac{\vec{d}_{des;i} \cdot v_{des;i} - \vec{v}_i(t)}{\tau} \tag{A4}$$

$$\vec{a}_{o;i}(t) = -a_w \sum_{o \in O} \vec{e}_{i;o} \begin{cases} 1 & \text{if } 0 < d_{i;o} \leq \frac{d_{shy}}{2} \\ 2\left(1 - \frac{d_{i;o}}{d_{shy}}\right) & \text{if } \frac{d_{shy}}{2} < d_{i;o} \leq d_{shy} \\ 0 & \text{otherwise} \end{cases} \tag{A5}$$

$$\vec{a}_{a;i}(t) = -a_0 \sum_{j \in A} \vec{e}_{i;j} \cdot e^{-d_{i;j}/r_0} \tag{A6}$$

Each time step, NOMAD updates the position of each pedestrian based on the acceleration of the pedestrian by integrating the acceleration twice using an Euler scheme (equations A1 and A2). The acceleration itself is computed using so-called social forces. Equation A3 presents the three forces that govern the acceleration and with that the movement. These are the following force ($\vec{a}_{f;i}$) that ensures the agent follows their preferred route to their destination, the object repulsions force ($\vec{a}_{o;i}$) that ensures agents avoid obstacles, and the agent repulsion force ($\vec{a}_{a;i}$) which ensures agents avoid collisions with other agents. $\vec{\xi}$ is the fluctuation term which simulates the natural fluctuation in the agents' movements. Equation A4 shows that the agent tries to match their current velocity ($\vec{v}_i(t)$) with their desired velocity ($\vec{d}_{des;i} \cdot v_{des;i}$) which is composed of their desired direction ($\vec{d}_{des;i}$) determined by the routing floor field and their desired speed ($v_{des;i}$). The τ parameter determines how strongly an agent reacts to any straying from their preferred velocity whereby the smaller the value of τ, the stronger the reaction. Equation A5 presents the force that acts upon an agent when they come close to one or more obstacles. If the distance between the agent and the closest point on an obstacle ($d_{i;o}$) is smaller than or equal to the shy away distance (d_{shy}), the pedestrian will experience a social force from this obstacle. The closer the pedestrian is to the obstacles, the larger the force. The relative strength of this force, compared to the other forces, is determined by the parameter a_w. $\vec{e}_{i;o}$ is the vector pointing from the agent to the closest point on the obstacle. The interaction between agents is governed by equation A6. For each agent in the set of other agents in the neighborhood (A), an agent experiences a repulsive force. The smaller the distance between the agent ($d_{i;j}$), the larger the force whereby r_0 governs how strongly an agent responds to this distance. The parameter a_0 determines how strong this agent's repulsion force is compared to the other forces. $\vec{e}_{i;j}$ is the vector pointing from the agent to the other agent.

Appendix C. Example Agent-Based Script

```
"name": "agent41",
            "script": {
                "49": {
                    "type": "enter",
                    "x": 85,
                    "y": 71,
                },
                "50": {
                    "type": "move",
                    "x": 39,
                    "y": -42,
                },
                "316": {
                    "type": "leave"
                }
```

This script indicates that the agent41 enters the venue at time 49 with the starting location of x:85, y:71, then by time 50, the agent moves in the direction x:39, y:-42, then stays in this location, and finally leaves the space at time 316.

Appendix D. Virus Spread and Transmission Model (QVEmod) Equations (adapted from Atamer Balkan & Chang et al., 2024)

Virus Emission: The virus emission rate that infectious agent i shed into the air per time is distributed over aerosols ($r^i_{emission-aerosols}$) and droplets ($r^i_{emission-droplets}$) (Eq. $A7$ and $A8$). Here, ω represents the unit emission rate at which a typical infectious individual i emits virus in unit time (i.e., one hour in our case) under half-time breathing and talking condition. η represents the proportion of pathogen excreted to hands, therefore $(1-\eta)$ represents the proportion emitted to the air. p_j represents the proportion of viruses emitted in the form of aerosols and droplets, where the two proportions ($p_{aerosols}$, $p_{droplets}$) add up to 1. The virus emission calculation is triggered only for the grid cell (x, y) in which the infectious agent is at time t; otherwise, it is 0.

$$r^i_{emission-aerosols}(x,y,t) = \omega(1-\eta)p_{aerosols} \tag{A7}$$

$$r^i_{emission-droplets}(x,y,t) = \omega(1-\eta)p_{droplets} \tag{A8}$$

Surface Contamination: An infectious individual is assumed to contaminate the surfaces they frequently touch (e.g., tables and chairs they use) within their reachable distance. The rate of surface contamination in grid cell (x, y) by the infectious individual i is defined by the touching frequency (γ), transfer efficiency (θ), and the ratio of finger pads surface relative to the reachable surface area (π) (Eq. $A9$). V^i_{hand} is initialized at t=0 as a proportion of emission rate ω, where η represents the proportion of pathogen excreted to hands (Eq. $A10$).

$$r^i_{contamination}(x,y,t) = V^i_{hand}(t)\gamma\theta\pi$$

$$V^i_{hand}(t) = V^i_{hand}(0) = \omega\eta$$

Virus Inhalation: The virus inhalation rates in the form of aerosols and droplets by the susceptible individual s ($r^s_{inhalation-aerosols}$, $r^s_{inhalation-droplets}$) are defined by the airborne viruses accumulated in the air in grid cell (x, y) that the susceptible agent is present at time t ($V_{aerosols}(x,y,t)$, $V_{droplets}(x,y,t)$), the unit inhalation rate of the individual (ρ) and the grid cell volume (L) (Eq. $A11$ and $A12$).

$$r^s_{inhalation-aerosols}(x,y,t) = V_{aerosols}(x,y,t)\frac{\rho}{L} \tag{A11}$$

$$r^s_{inhalation-droplets}(x,y,t) = V_{droplets}(x,y,t)\frac{\rho}{L} \tag{A12}$$

Virus Pick-up from the Surfaces: The virus transfer from contaminated surfaces to hands occurs when a susceptible individual s touches the contaminated surfaces in grid cells (x, y) within their reachable distance. Similar to the surface contamination process, the virus pick-up rate ($r^s_{pick-up}$) is defined by the virus accumulated on surfaces in grid cell (x, y) at time t ($V_{fomites}(x,y,t)$), the touching frequency (γ), transfer efficiency (θ), and the ratio of finger pads relative to the reachable surface area (π) (Eq. $A13$ and A14). As the virus transfer from surfaces to hands occurs, it is assumed that the virus accumulates in each susceptible agent's hands, V^s_{hand} (Eq. $A15$).

$$r^s_{pick-up}(x,y,t) = V_{fomites}(x,y,t)\gamma\theta\pi \tag{A13}$$

$$r^s_{pick-up}(t) = \sum_{x,y} r^s_{pick-up}(x,y,t) \tag{A14}$$

$$V^s{}_{hand}(t+\Delta t) = V^s{}_{hand}(t) + r^s{}_{pick-up}(t)\Delta \mathrm{t} \tag{A15}$$

Virus Exposure: For each susceptible agent s, the accumulated virus exposure via aerosols and droplets, $E^s{}_{aerosols}(T)$ and $E^s{}_{droplets}(T)$, are calculated by the summation of the inhaled amount of viruses up to time T (Eq. $A16$ and $A17$). The exposure from fomites route up to time T, $E^s{}_{fomites}(T)$, is calculated as a proportion of viruses on hands that are assumed to be transferred from hands to facial membranes, ε (Eq. $A18$).

$$E^s{}_{aerosols}(T) = \sum_{t=0}^{t=T} \sum_{x,y} r^s{}_{inhalation-aerosols}(x,y,t) \tag{A16}$$

$$E^s{}_{droplets}(T) = \sum_{t=0}^{t=T} \sum_{x,y} r^s{}_{inhalation-droplets}(x,y,t) \tag{A17}$$

$$E^s{}_{fomites}(T) = \sum_{0}^{T} V^s{}_{hand}(t)\varepsilon\Delta t \tag{A18}$$

Virus Decay: Viral particles are assumed to decay exponentially in the environment, the rates of which vary in aerosols and on different surface materials. Virus-laden aerosols lose infectivity at a constant rate while floating in the air, and the air change rate (ACH) indoors has an increasing impact on their decay. The aerosols decay ($r_{decay-aerosols}$) and fomites decay ($r_{decay-fomites}$) equations for grid cell (x,y) at time t are identified as exponential decay functions where $\mu_{aerosols}$ and $\mu_{fomites}$ represent the unit decay rate of viruses in aerosols and on fomites respectively (Eq. $A19$ and $A20$).

$$r_{decay-aerosols}(x,y,t,\Delta t) = V_{aerosols}(x,y,t)\left(1 - e^{-\mu_{aerosols}\Delta t - ACH\Delta t}\right) \tag{A19}$$

$$r_{decay-fomites}(x,y,t,\Delta t) = V_{fomites}(x,y,t)\left(1 - e^{-\mu_{fomites}\Delta t}\right) \tag{A20}$$

Droplet Deposition: Viral-laden droplets can fall onto surfaces through sedimentation and can accumulate on the surfaces as fomites. The rate of viruses transferring from droplets onto fomites ($r_{deposition}$) for cell (x,y) at time t is defined by the unit deposition rate of viral-laden droplets ($\mu_{droplets}$) (Eq. $A21$).

$$r_{deposition}(x,y,t) = V_{droplets}(x,y,t)\mu_{droplets} \tag{A21}$$

Diffusion: The diffusion of the virus-laden particles in the air is defined by two-dimensional diffusion equations for aerosols and droplets. It is assumed that all particles are well-mixed in the volume of the grid cell, and they diffuse in (x,y) directions (Eq. $A22$ and $A23$) ("aerosols" and "droplets" are abbreviated as "a" and "d" respectively). Here, Δx and Δy represent the length unit of the cell (both 0.5m in the default), and D is the diffusion coefficient, indicating the unit diffusion rate per time.

$$r_{diffusion-aerosols}(x,y,t) = D\frac{(V_a(x-\Delta x,y,t)+V_a(x+\Delta x,y,t)+V_a(x,y-\Delta y,t)+V_a(x,y+\Delta y,t)-4V_a(x,y,t))}{\Delta x\Delta y} \tag{A22}$$

$$r_{diffusion-droplets}(x,y,t) = D\frac{(V_d(x-\Delta x,y,t)+V_d(x+\Delta x,y,t)+V_d(x,y-\Delta y,t)+V_d(x,y+\Delta y,t)-4V_d(x,y,t))}{\Delta x\Delta y} \tag{A23}$$

Virus Contamination States: In each time step Δt, $V_{aerosols}$ is decreased by the inhaled amount by the susceptible agents in grid cell (x,y), updated by the diffused amount of particles, decreased by the decay of viruses and increased by the virus emission if there exists an infectious agent in cell (x,y) at time t (Eq. $A24$). Similarly, $V_{droplets}$ is decreased by the inhaled amount by the susceptible agents in grid cell (x,y), updated by the diffused amount of particles, decreased by the deposition of viruses from air layer to surface layer, and increased by the virus emission if there exists infectious agent in cell (x,y) at time t (Eq. $A25$). In the surface layer, is decreased by the picked-up amount by the susceptible agents within the reachable distance to grid cell (x,y), increased by the deposition of viruses from air layer to surface layer, decreased by the decay of viruses on the surfaces and increased by the virus contamination if there exists an infectious agent within the reachable distance to grid cell (x,y) at time t (Eq. $A26$).

$$\begin{aligned} V_{aerosols}(x,y,t+\Delta t) &= V_{aerosols}(x,y,t) - \sum_s r^s{}_{inhalation-aerosols}(x,y,t)\Delta t \\ &+ r_{diffusion-aerosols}(x,y,t)\Delta t - r_{decay-aerosols}(x,y,t,\Delta t) + r^i{}_{emission-aerosols}(x,y,t)\Delta t \end{aligned} \tag{A24}$$

$$\begin{aligned} V_{droplets}(x,y,t+\Delta t) &= V_{droplets}(x,y,t) - \sum_s r^s{}_{inhalation-droplets}(x,y,t)\Delta t \\ &+ r_{diffusion-droplets}(x,y,t)\Delta t - r_{deposition}(x,y,t)\Delta t + r^i{}_{emission-droplets}(x,y,t)\Delta t \end{aligned} \tag{A25}$$

$$\begin{aligned} V_{fomites}(x,y,t+\Delta t) &= V_{fomites}(x,y,t) - \sum_s r^s{}_{pick-up}(x,y,t)\Delta t \\ &+ r_{deposition}(x,y,t)\Delta t - r_{decay-fomites}(x,y,t,\Delta t) + r^i{}_{contamination}(x,y,t)\Delta t \end{aligned} \tag{A26}$$

Appendix E. Causal Loop Diagram (CLD) for the relationships between the processes in QVEmod and the viral particles in a grid cell (x,y)

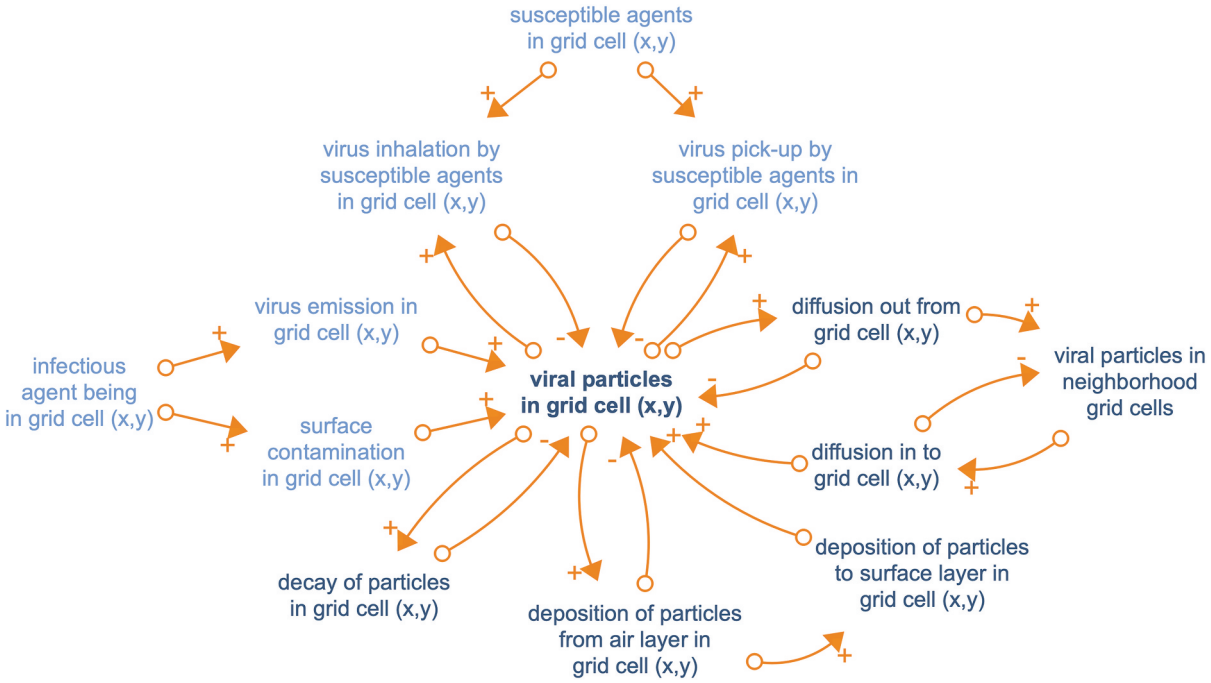

Figure A1. CLD for virus spread and transmission processes in QVEmod. (Agent-triggered variables are shown with light blue, whereas the environment-related variables are shown with dark blue.)

Appendix F. Model Verification and Validation

Model verification and validation were conducted as integrated stages of the simulation modeling process. In the initial phases of the project, the workshops carried out with the social venue owners and domain experts have contributed to the ***conceptual model validation***. In the further stages, the ***model verification*** was iteratively conducted for each section of the model, testing if the computer models represent the conceptual model and if the model software performs as it intends. In line with the model verification steps, we conducted structural validity tests (Barlas, 1996) such as *dimensional consistency tests* (i.e., checking whether the right-hand side and left-hand side of each equation in QVEmod is dimensionally consistent) and *extreme condition tests* (i.e., checking if an extreme condition results in anticipated behavior (e.g., what if there were only one guest but several service personnel)). For the integrated hybrid model, *integration error tests* have been conducted to select the best value for delta time, Δt, considering the rate of the processes in the model (e.g., for a given grid cell size, Δt should be small enough to capture the airflow between grid cells). Then, we performed the ***scenario verification*** and ***operational validation*** tests for the model in an integrated manner. The behavior of the activity choice and scheduling model has been studied and face validation has been performed (Sparnaaij et al., 2024). The NOMAD model has been extensively calibrated and validated in the context of general walking behavior of pedestrians (Campanella et al., 2009; Campanella et al., 2014; Campanella, 2016). Face validity of the virus spread and exposure calculations has been assessed by means of workshops with virologists and epidemiologists. Then, for the integrated hybrid model, a series of sensitivity analysis has been conducted, especially for the parameters related to virus characteristics and biological and physical processes (Atamer Balkan & Chang et al., 2024). Due to a lack of reference observational and complete data sets, a formal statistical validity test was not possible. Yet, the route-specific exposure parameters $k_{aerosols}$, $k_{droplets}$ and $k_{fomites}$ in the dose-response function (Eq.1), which are generally hard to quantify even with experiments (Watanabe et al. 2010; Callaway 2020), were aligned using the available empirical data, so that the model outputs are in line with real-world observations. Specifically, the base case restaurant simulation scenario in Atamer Balkan and Chang (2024) is considered and those values for $k_{aerosols}$, $k_{droplets}$ and $k_{fomites}$ that provided the best agreement ($R_{event} = 0.81$) with the observed SARS-CoV-2 outbreak clusters in similar social settings reported in Adam et al. (2020) ($R_{event} = 0.80$) are selected. The sensitivity of model results to these assumptions is presented in Atamer Balkan and Chang (2024). The simulations should thus be considered to represent the case for the wild-type SARS-CoV-2 virus, although adaptations to other respiratory viruses can be made provided sufficient empirical support.

Appendix G. Simulation Run Time

For these experiments, the simulation running time is 10-12 minutes for each replication of Pedestrian Behavior and Mobility model and 0.5 minutes for each replication of QVEmod on a computer having a configuration of 2.3 GHz 8-Core Intel Core i9 processor and 16 GB 2667 MHz DDR4 memory.

Appendix H. Infection Prevalence and $p - in_{event}$

Infection prevalence represents the proportion of infectious individuals within a community. For our example case, we refer to the infection prevalence in the Netherlands around late January 2022, just after when the restaurants were reopened and allowed to be open until 22:00 on January 26, 2022.

After this regulation went into effect, the 7-day average number of confirmed cases in the Netherlands changed between 54,710 - 67,495 from January 26 to January 31, with an average of 60,197 (RIVM Coronavirus Dashboard, accessed on May 2022, URL: https://coronadashboard.government.nl/landelijk/positief-geteste-mensen). We assume that the number of actual cases is twice the number of confirmed cases. On average, we assume that an infected person can stay infectious for 7 days. The population of the Netherlands during this period was projected to be 17,597,607 (CBS Netherlands, accessed on May 2022, URL: https://opendata.cbs.nl/statline/#/CBS/nl/dataset/37230ned/table). Then, the average infection prevalence is calculated as follows:

$$\text{infection prevalence} = p - in = (60,197 \times 2 \times 7)/17,597,607 = 4.8\%$$

However, for our calculations, we need $p - in_{event}$, the "the proportion of infectious individuals who do not have severe symptoms so that they can show up in a social space". That is, they are either asymptomatic (i.e., do not show symptoms) with a chance of 20% (Buitrago-Garcia et al., 2020) or they are symptomatic, but they are at the first phase (i.e., first day) of their infectious period and do not have severe symptoms:

$$\text{infection prevalence in social spaces} = p - in_{event} = p - in \times (0.2 \times (7/7) + 0.8 \times (1/7)) = 1.5\%$$

Appendix I. Adaptability of PeDViS to Other Indoor Spaces and Respiratory Pathogens

Owing to the modular setup of PeDViS, it can be used to characterize the infection risks in other types of indoor spaces with different human movement and behavior characteristics. For the agent movement, NOMAD is a general-purpose pedestrian simulation model and applicable across diverse contexts. It is thus not specific to restaurants but can be applied to various indoor spaces like office spaces (Deijkers, 2022) as well as outdoor events such as festivals (Wang, 2021). To tailor NOMAD to specific settings, one needs to define the relevant infrastructure. This entails specifying the location of all obstacles, activities, and points of entry and exit for pedestrians. For instance, for the case of a supermarket or store (demonstrated in Figure A2), the layout needs to be modified to accommodate relevant infrastructural elements (Section 2.1), particularly store racks as 'obstacles' so that neither the agents nor the viral particle can move through the racks. Additionally, it is necessary to define the pedestrian profile parameters (Section 2.2.2.1) for characterizing the pedestrian walking behavior, representing differences in population and behavior between, for example, an office space and a retail store.

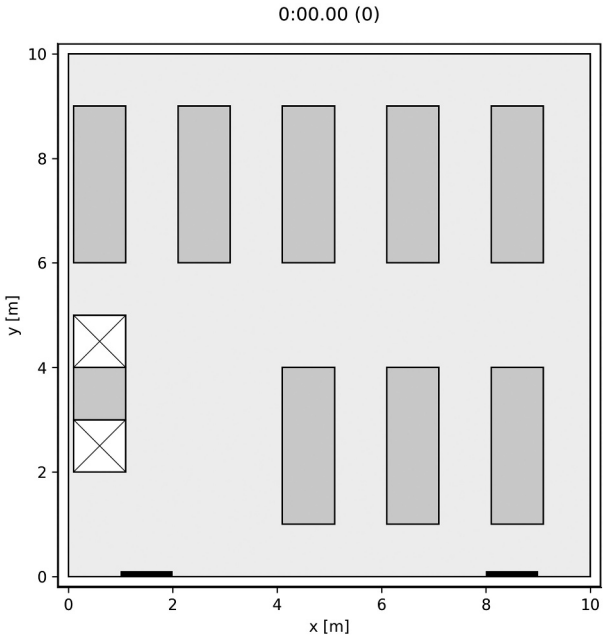

Figure A2. Visual representation of an example 10x10 m2 retail store, with eight store racks, one register for payment (on the left) and doors for entry and exit (on the bottom)

The activity choice and scheduling module, on the other hand, requires larger adaptation when applied in different contexts. Currently, the model features a tailor-made activity choice and scheduling module for both customers and personnel in a restaurant environment (Section 2.2.1.1). For any other context, one must either input a predefined activity schedule for each pedestrian (or pedestrian group) or implement an existing or a new activity choice and scheduling module tailored to the specific context. Deijkers (2022) and Wang (2021) demonstrate the application of the latter approach for office environments and festival grounds, respectively. For example, in a supermarket context, a different activity choice and scheduling behavior for the customers (and personnel) is required. The basic behavior would include customers entering the supermarket, walking to N different locations within, waiting there for a short time to get their products from the racks, proceeding to the check-out, queueing if necessary, waiting at the pay register to simulate the check-out process, and exiting the supermarket.

The model can also be adapted to different SARS-CoV-2 variants and other respiratory pathogens by adjusting relevant model parameters. In Atamer Balkan and Chang et al. (2024), the data requirements and analyses needed to parameterize and calibrate the model for the wild-type SARS-CoV-2 virus are outlined. Adapting to other variants or respiratory pathogens requires careful consideration of the core mechanisms that underlie differences in transmission potential. For instance, subsequent SARS-CoV-2 variants often outcompete earlier variants by being more successful at evading the immune response. In QVEmod, the altered susceptibility of the recipient host (i.e., probability of acquiring infection upon exposure) is captured in the dose-response relationship (Eq.1, Section 2.2.3.3). To incorporate a change in the susceptibility of individuals, the functional form of the dose-response curve (Eq.1, Section 2.2.3.3) and its parameters can be readjusted. Other indicators for biological mechanisms could also underlie the difference in transmission between respiratory pathogens (or variants of the same pathogen), including the parameters reflecting the virus emission characteristics of the infectious individuals (Section 2.2.2.1), and virus spread-related parameters in decay, deposition, and diffusion processes (Section 2.2.2.2). Consultation with experts in virology and immunology is important for the correct interpretation of the experimental data used to inform these mechanisms. Lastly, insofar as epidemiological data is available on (the distribution of) outbreak clusters in indoor settings, these could be used to validate model outcomes. In doing so, one ensures that the implemented changes at the level of virus-host and virus-environment interactions indeed result in the observed epidemiological patterns.